HAL
open science

X-FEM in isogeometric analysis for linear fracture mechanics

Emmanuel de Luycker, David J. Benson, Ted Belytschko, Yuri Bazilevs, Ming Chen Hsu

To cite this version:

Emmanuel de Luycker, David J. Benson, Ted Belytschko, Yuri Bazilevs, Ming Chen Hsu. X-FEM in isogeometric analysis for linear fracture mechanics. International Journal for Numerical Methods in Engineering, 2011, 87 (6), pp.541-565. 10.1002/nme.3121 . hal-01657905

HAL Id: hal-01657905

https://hal.science/hal-01657905v1

Submitted on 7 Dec 2017

HAL is a multi-disciplinary open access archive for the deposit and dissemination of scientific research documents, whether they are published or not. The documents may come from teaching and research institutions in France or abroad, or from public or private research centers.

L'archive ouverte pluridisciplinaire **HAL**, est destinée au dépôt et à la diffusion de documents scientifiques de niveau recherche, publiés ou non, émanant des établissements d'enseignement et de recherche français ou étrangers, des laboratoires publics ou privés.

Open Archive Toulouse Archive Ouverte (OATAO)
OATAO is an open access repository that collects the work of Toulouse researchers and makes it freely available over the web where possible.

This is an author-deposited version published in: http://oatao.univ-toulouse.fr/
Eprints ID: 18482

To link to this article: DOI:10.1002/nme.3121/full
URL:http://onlinelibrary.wiley.com/doi/10.1002/nme.3121/full

To cite this version:

De Luycker, Emmanuel and Benson, David J. and Belytschko, Ted and Bazilevs, Yuri and Hsu, Ming Chen *X-FEM in isogeometric analysis for linear fracture mechanics.* (2011) International Journal for Numerical Methods in Engineering, vol. 87 (n° 6). pp. 541-565. ISSN 1097-0207

Any correspondence concerning this service should be sent to the repository administrator: staff-oatao@listes-diff.inp-toulouse.fr

X-FEM in isogeometric analysis for linear fracture mechanics

E. De Luycker[1,2,*,†], D. J. Benson[1], T. Belytschko[2], Y. Bazilevs[1] and M. C. Hsu[1]

[1]*Department of Structural Engineering, University of California San Diego, 9500 Gilman Drive, La Jolla, CA 92093, U.S.A.*
[2]*Department of Mechanical Engineering, Northwestern University, Evanston, IL 60280, U.S.A.*

SUMMARY

The extended finite element method (X-FEM) has proven to be an accurate, robust method for solving problems in fracture mechanics. X-FEM has typically been used with elements using linear basis functions, although some work has been performed using quadratics. In the current work, the X-FEM formulation is incorporated into isogeometric analysis to obtain solutions with higher order convergence rates for problems in linear fracture mechanics. In comparison with X-FEM with conventional finite elements of equal degree, the NURBS-based isogeometric analysis gives equal asymptotic convergence rates and equal accuracy with fewer degrees of freedom (DOF). Results for linear through quartic NURBS basis functions are presented for a multiplicity of one or a multiplicity equal the degree. Copyright © 2011 John Wiley & Sons, Ltd.

KEY WORDS: X-FEM; isogeometric analysis; NURBS; linear fracture mechanics

1. INTRODUCTION

Dynamic crack propagation is a major challenge for structural analysis due to the singularity at the crack tip, and the propagation of a crack adds the challenge of modifying a Lagrangian mesh to accommodate the evolving geometry. Several numerical methods have been developed during the past decade to address these issues, and most build on the classical finite element method (FEM). Arbitrary Lagrangian–Eulerian formulations [1] and re-meshing [2] are standard approaches to extending FEM to a dynamically changing domain. Both the methods are time consuming and complicated because of the necessity to go back to the geometry definition in one case and because of the convection step in the other. One alternative to re-meshing is the use of meshless methods [3–5]. Another is the extended FEM (X-FEM) [6, 7] which allows modeling cracks with an incompatible mesh through the introduction of discontinuous-enrichment functions [7]. Coupled with the level set method, X-FEM provides a mean for propagating cracks without remeshing [8]. Optimal convergence rates are obtained by introducing tip-enrichment functions from the asymptotic crack tip displacement field [9]. The accuracy of the stress-intensity factor can also be improved by combining a meshfree formulation with the crack tip enrichment [10].

Non-uniform rational B-splines (NURBS) are widely used in computer aided design (CAD) because of their ability to exactly represent complex geometries. *Isogeometric analysis* uses the same functions for analysis [11], eliminating the traditional intermediate step of mesh generation for FEM. This bridge between CAD and numerical simulation permits an exact description of the

*Correspondence to: E. De Luycker, Department of Structural Engineering, University of California San Diego, San Diego, 9500 Gilman Drive, La Jolla, CA 92093, U.S.A.
†E-mail: Emmanuel.De-Luycker@ens-cachan.org

geometry even on coarse meshes. The solution refinement procedure, analogous to adaptivity (h and p-refinement methods), is enhanced as well with the introduction of k-refinement [11]. NURBS basis functions avoid dealing with the geometrical approximations of classical finite element (FE) meshes. They also possess the higher order continuity required for a rotation-free shell formulation [12], permit explicit time integration with higher order elements without the usual FEM stable time step size penalty [13], and generally add robustness to the computations [14]. NURBS are attractive in various fields of mechanics, from turbulence and fluid–structure interaction [15–17] to incompressible problems [18] or digital image correlation [19].

In this paper we propose an isogeometric formulation using NURBS basis functions that are enriched via X-FEM to solve linear fracture mechanics problem with incompatible meshes. Section 1 briefly reviews the isogeometric and X-FEM concepts. The reference problem is described in Section 2 along with two methods for accurately imposing the boundary conditions with the NURBS basis functions and the crack-enrichment functions. Convergence is verified for the imposed Dirichlet conditions. The X-FEM formulation with strongly discontinuous enrichment functions and NURBS is described in Section 3; different support options for the enrichment are tested and a solution is outlined concerning the choice of this support. A singular enrichment is introduced in Section 4 from the theoretical asymptotic solution from mode I linear fracture, and different compatibility techniques are discussed. The proposed method reaches optimal convergence for linear through quartic NURBS shape functions with a multiplicity of 1 or equals to the degree, and the NURBS functions are more accurate in terms of DOF compared with the FE basis functions. Some conclusions and perspectives are given in Section 5. Finally, the *generalized element* formulation [13] used to investigate the solutions and perform the computations is briefly described in the Appendix.

1.1. Non uniform rational B-Splines (NURBS)

The classical FEM builds a continuous approximation from the interpolation of a set of nodal values as illustrated by Equation (1), where s is a coordinate in the parametric space, N_A is the Lagrange or serendipity basis function associated with node A, and $\boldsymbol{x}_A$ are the nodal coordinates; $\mathcal{N}$ are all the indices of the basis functions on the computational mesh:

$$\boldsymbol{x}(s,t)=\sum_{A\in\mathcal{N}} N_A(s)\boldsymbol{x}_A(t) \tag{1}$$

This contribution to $\boldsymbol{x}$ will be called the *classical* part of the approximation in the remainder of the paper regardless of whether Lagrangian polynomials or NURBS are used.

Because of the partition of unity and the *Kronecker-delta* property in Equation (2), the approximate field interpolates the nodes: $\boldsymbol{x}(s^A)=\boldsymbol{x}_A$:

$$N_A(s^B)=\boldsymbol{\delta}_{AB} \tag{2}$$

The boundary conditions are therefore easy to impose because each node is located in the problem domain. The nodes are directly driven with a displacement equal to the desired displacement field (depending only on the position of the node) to impose Dirichlet boundary conditions.

In this paper, we consider a set of basis functions widely used in CAD, and recently introduced for computational mechanics [11], called NURBS. Some examples of NURBS basis functions are presented in Figure 1 for 5 elements with various orders of multiplicity in the *knot vector*. The term *element* deserves here a clarification; in the classical FEM, each element refers to a single 'parent element' or 'reference element' with its own parametric variables in $[-1,1]$ or $[0,1]$ depending on the kind of element considered. An integration strategy is then defined and applied for each element. With NURBS, the definition of an element describes as well the unique integration strategy (when a discontinuity is not present), but the notion of parent element no longer exists. However, with NURBS, the elements are intimately linked to the knot vector as they are defined as the interval between two distinct adjacent knot values. In Figure 1, the basis functions related to 5 elements are illustrated. When the multiplicity equals the degree in Figures 1(a) and (c), a pattern can be determined as in the FEM, but in Figures 1(b) and (d), if the number

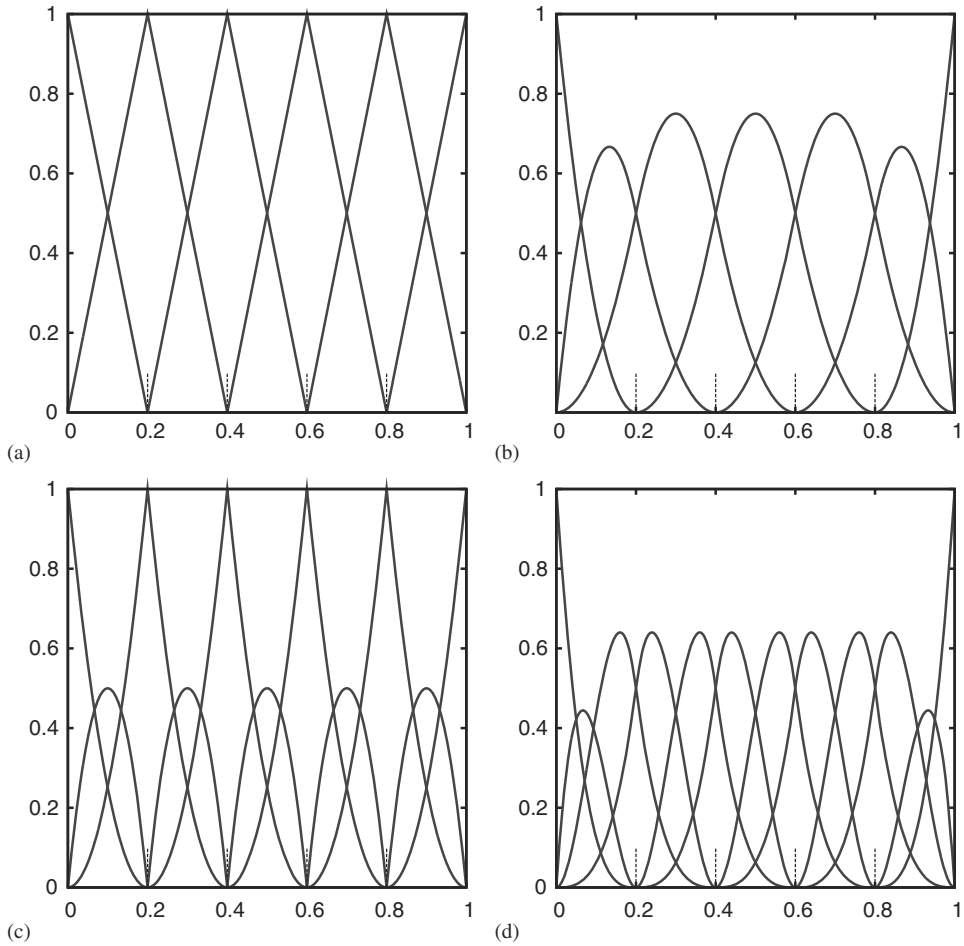

Figure 1. One-dimensional basis functions for 5 elements on the parametric domain. (a) $\Xi = [0, 0, .2, .4, .6, .8, 1, 1]$ degree 1, multiplicity equal to 1; (b) $\Xi = [0, 0, 0, .2, .4, .6, .8, 1, 1, 1]$ degree 2, multiplicity equal to 1; (c) $\Xi = [0, 0, 0, .2, .2, .4, .4, .6, .6, .8, .8, 1, 1, 1]$ degree 2, multiplicity equal to 2; (d) $\Xi = [0, 0, 0, 0, .2, .2, .4, .4, .6, .6, .8, .8, 1, 1, 1, 1]$ degree 3, multiplicity equal to 2.

of basis functions still equals the degree plus one, a single 'parent elements' cannot be extracted. The main advantages of these basis functions are:

- Their use in CAD shortens the design-to-analysis process by reducing or eliminating the mesh generation time, the most time-consuming step in the FE analysis.
- The ability to exactly represent basic geometries like circles even with coarse meshes.
- The higher order continuity of the basis functions, which is generally C^{p-1} where p is the degree of the basis function. For example, quadratic NURBS are C^1 continuous across the mesh.

An approximate solution can then be constructed using these basis functions:

$$\boldsymbol{x}(s,t) = \sum_{A \in \mathcal{N}} N_A(s) \boldsymbol{q}_A(t) \tag{3}$$

NURBS do not fulfill the *Kronecker-delta* property in Equation (2), and therefore the *control points* are no longer called nodes because they generally are not points in the problem domain, and the location of a control point is denoted by $\boldsymbol{q}$ to emphasize this property. Using open knot vectors ensures the *Kronecker-delta* property in the extremum points which simplify the imposition

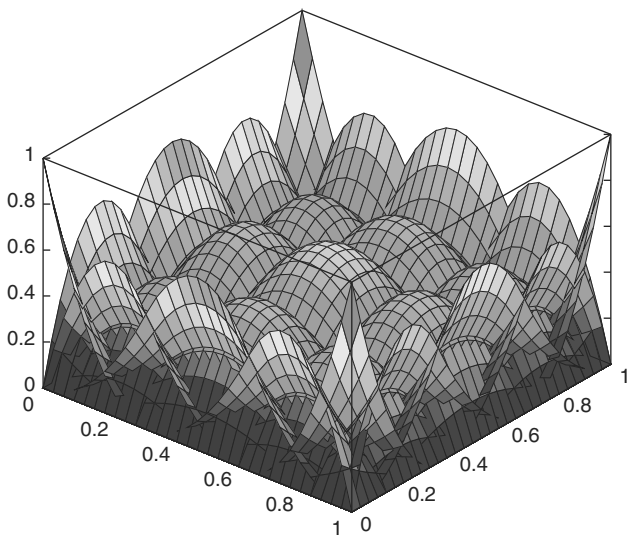

Figure 2. Bivariate, degree 2 NURBS basis functions for 5×5 elements and a knot vector: $\Xi\times\Theta=[0,0,0,.2,.4,.6,.8,1,1,1]\times[0,0,0,.2,.4,.6,.8,1,1,1]$.

of boundary conditions in most cases. The parametrization is defined via the knot vector and the multiplicity of each knot value may change locally, and therefore alter locally the continuity of the approximation. In general, for NURBS of degree p with a multiplicity of n at knots, the derivatives are continuous up to order $p-n$. Examples in Figures 1(a) and (c) illustrate that when the knot multiplicity equals the degree of the basis functions that C^0 interfaces are introduced between the elements. In this particular case, the NURBS basis functions are close to the Lagrange polynomial basis functions classically used in the FEM because the control points interpolate the solution on the sides (or the corners) of the elements and span the same approximation space within the elements. This particular knot vector with a uniform knot multiplicity that equals the degree will be called FE solution while the NURBS solution will refer to a multiplicity of 1 in the knot vector. The two-dimensional span of the basis functions, generated from an outer product, is illustrated in Figure 2 for 5×5 quadratic elements.

1.2. The extended finite element method (X-FEM)

The accuracy of the FEM for singular problems may be increased, and its convergence rate improved, by adding additional basis functions to the solution space provided they satisfy the requirements set forth by the partition of unity method (PUM) [20]. In practice, the classical solution (Equation (1) for FE and (3) for NURBS) is usually enhanced with a set of enrichment functions motivated by the form of the analytical solution for a model problem. The analytical function ϕ, for example, may be introduced in Equation (4) using a set of basis functions $\widetilde{N}$ to build a partition of unity. The enrichment can be restricted to a specific area with X-FEM [6, 7] to improve efficiency. In general, the $\widetilde{N}$ basis functions are different from the ones used for the classical solution. For higher order basis functions, a linear $\widetilde{N}$ may be preferred [21, 22]. The indices of the basis functions used for the enrichment are denoted as $\mathscr{S}$ and $\widetilde{\boldsymbol{x}}$ are the (few) additional DOF associated with them:

$$\boldsymbol{x}(\boldsymbol{s},t)=\sum_{A\in\mathscr{N}}N_A(\boldsymbol{s})\boldsymbol{x}_A(t)+\phi(\boldsymbol{s})\sum_{A'\in\mathscr{S}}\widetilde{N}_{A'}(\boldsymbol{s})\widetilde{\boldsymbol{x}}_{A'}(t) \tag{4}$$

The analytical field ϕ can take many forms, and the range of application for X-FEM is wide, ranging from crack growth simulations without re-meshing [6] to contact problems in multi-material

arbitrary Lagrangian Eulerian formulations [23]. Typical enrichment functions used in X-FEM are:

- The Heaviside function H, defined in Equation (23), was used in [24] for meshless methods. This step function introduces a strong discontinuity in the solution, and permits cracks incompatible with the mesh. We will use this enrichment in Section 3 with NURBS.
- The distance function that introduces a weak discontinuity in the displacement for multi-material problems with discontinuous material properties and shear band formation.
- The singular asymptotic field near the tip of a crack, Equation (11). This enrichment will be used in Section 4 for mode I linear fracture analysis.

An detailed review of the X-FEM method can be found in [25].

1.3. X-FEM with NURBS

NURBS are particularly suitable for problems with smooth solutions because of their higher order continuity. By introducing X-FEM enrichment functions, the advantages of X-FEM and isogeometric analysis are combined: complex geometries are represented exactly and accurate solutions are obtained for discontinuous or singular problems with only a few additional DOF. Using the NURBS basis functions and the corresponding control points with X-FEM gives

$$\boldsymbol{x}(s,t)=\sum_{A\in\mathscr{N}} N_A(s)\boldsymbol{q}_A(t)+\phi(s)\sum_{A'\in\mathscr{S}} \widetilde{N}_{A'}(s)\widetilde{\boldsymbol{q}}_{A'}(t) \tag{5}$$

The subscript A' in $\mathscr{S}$ refers to the enriched basis functions. The choice of the enriched subdomain will be discussed later. Two techniques, *blending* and the *shifting*, are commonly used to guarantee compatibility between the enriched and the un-enriched subdomains. These techniques are discussed in Sections 3.2 and 4.2.

2. THE MODEL PROBLEM—A CRACK IN AN INCOMPATIBLE MESH

The model problem consists of a square domain with a crack running from the middle of the left boundary to the center of the domain. Displacement boundary conditions consistent with the asymptotic solution for a pure mode I crack are imposed. The crack faces are traction free and there are no imposed displacement boundary conditions on them. An odd number of elements are used in the vertical direction so that the crack runs down the middle row of elements.

2.1. The governing continuum equations

The problem domain Ω is subjected to body forces $\boldsymbol{b}_d$, imposed displacements $\boldsymbol{U}_d$ on section of the boundary denoted $\partial\Omega_1$ and imposed tractions $\boldsymbol{F}_d$ on the complementary $\partial\Omega_2$ (so that $\partial\Omega_1 \bigoplus \partial\Omega_2=\partial\Omega$). The crack in Ω is traction free, making the two faces of the crack part of $\partial\Omega_2$ with $\boldsymbol{F}_d=0$. The strong form of the momentum equation is given by

$$\nabla.\boldsymbol{\sigma}+\boldsymbol{b}_d=\rho\ddot{\boldsymbol{x}} \quad \text{in } \Omega \tag{6}$$

where $\nabla.$ is the divergence operator, $\boldsymbol{\sigma}$ the Cauchy stress tensor, ρ the density, and $\ddot{\boldsymbol{x}}$ is the acceleration. The boundary conditions are given by:

$$\boldsymbol{u}=\boldsymbol{U}_d \text{ on } \partial\Omega_1, \quad \boldsymbol{\sigma}.\boldsymbol{n}=\boldsymbol{F}_d \quad \text{on } \partial\Omega_2 \tag{7}$$

The mechanical behavior of the material is governed by a linear elastic constitutive law where $\boldsymbol{C}$ is the Hookean elastic tensor, λ and μ are the Lamé coefficients:

$$\boldsymbol{\sigma}=\boldsymbol{C}:\epsilon=\lambda tr(\epsilon)\boldsymbol{I}+2\mu\epsilon \tag{8}$$

The infinitesimal strain tensor is the symmetric part of the displacement gradient,

$$\epsilon=\tfrac{1}{2}(\nabla\boldsymbol{u}+\nabla^T\boldsymbol{u}) \tag{9}$$

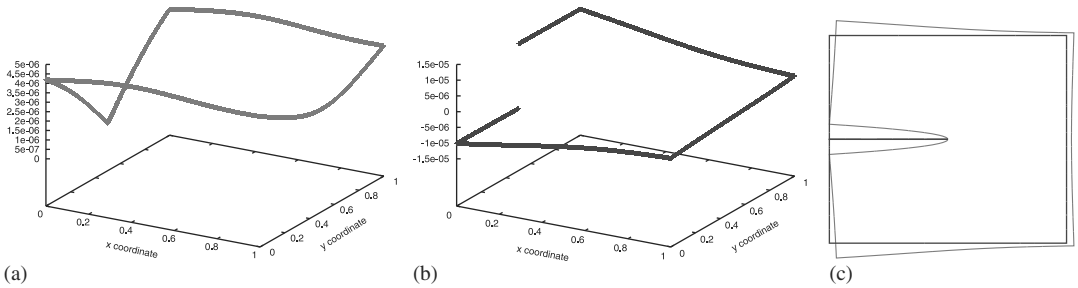

Figure 3. Displacement on the boundary of the domain for pure mode I and a stress-intensity factor $K_1 = 100$. (a) X displacement; (b) Y displacement; and (c) magnified deformation

The corresponding weak form, Equation (10), is obtained multiplying Equation (6) with a virtual displacement $\boldsymbol{u}^* \in \mathscr{U}_0$, $\mathscr{U}_0 = \{\boldsymbol{u}, \boldsymbol{u} = 0 \text{ on } \partial\Omega_1\}$, the homogeneous space associated with the admissible displacements space $\mathscr{U} = \{\boldsymbol{u}, \boldsymbol{u} = \boldsymbol{U}_d \text{ on } \partial\Omega_1\}$, then integrating over the volume Ω, and using the divergence theorem.

$$\int_\Omega \boldsymbol{\sigma} : \epsilon(\boldsymbol{u}^*)\,\mathrm{d}\Omega = \int_\Omega (\boldsymbol{b}_d - \rho\ddot{\boldsymbol{x}}).\boldsymbol{u}^*\,\mathrm{d}\Omega + \int_{\partial\Omega_2} \boldsymbol{F}_d.\boldsymbol{u}^*\,\mathrm{d}S \quad \forall \boldsymbol{u}^* \in \mathscr{U}_0 \tag{10}$$

2.2. Asymptotic analytical solution for pure mode I fracture

The asymptotic field near the tip in pure mode I is given in polar coordinates centered at the crack tip by Equation (11), where r is the distance to the tip and θ is the signed angle to the direction of propagation of the crack.

$$\boldsymbol{u}^{\infty}_{K_1}(r,\theta) = \frac{\sqrt{r}}{2\sqrt{2\pi}\mu}\begin{bmatrix} \left(-\frac{1}{2}+k\right)\cos\frac{\theta}{2} - \cos\frac{3\theta}{2} \\ \left(\frac{1}{2}+k\right)\sin\frac{\theta}{2} - \sin\frac{3\theta}{2} \end{bmatrix} \tag{11}$$

with $k = 3 - 4\nu$ for plane strain and $k = (3-\nu)/(1+\nu)$ for plane stress. The corresponding displacement for a stress-intensity factor K_1 is

$$\boldsymbol{u}(r,\theta) = \boldsymbol{u}^{\infty}_{K_1}(r,\theta)K_1 \tag{12}$$

The X and Y components of the imposed displacements are shown in Figures 3(a) and (b), and the distorted geometry in Figure 3(c).

2.3. Boundary displacements imposition

Since NURBS, like most meshfree basis functions, do not satisfy the Kronecker-delta property, driving the control points according to their coordinates, in contrast to nodes with Lagrange basis functions, may not be accurate enough in some high-performance applications. In many cases such as a rigid motion imposition or clamping a portion of the domain, Dirichlet boundary conditions may be applied directly especially when combined with open knot vectors. Nevertheless, when dealing with complicated fields, and when accuracy is a main concern, some specific techniques have to be used. Two different approaches for imposing arbitrary Dirichlet boundary conditions were evaluated:

- *Interpolating points* were introduced as linear functions of the control points. They were driven by the displacement of those points based on their spatial location with Equation (12).
- The control point displacements are calculated by minimizing an approximation of the L_2 displacement error on the boundary.

2.3.1. Interpolating points. Given a set of m points chosen on the boundary of the domain (equal to n, the number of control points involved in the boundary condition), a linear system can be written in a matrix form after renumbering the associated N and $\boldsymbol{q}$ from 1 to n,

$$\begin{pmatrix} N_1^1 & \dots & N_n^1 \\ \vdots & \ddots & \vdots \\ N_1^m & \dots & N_n^m \end{pmatrix} \begin{pmatrix} q_x^1 & q_y^1 & q_z^1 \\ \vdots & \vdots & \vdots \\ q_x^n & q_y^n & q_z^n \end{pmatrix} = \begin{pmatrix} x_x^1 & x_y^1 & x_z^1 \\ \vdots & \vdots & \vdots \\ x_x^m & x_y^m & x_z^m \end{pmatrix} \tag{13}$$

where $N_A(s^m)$ is denoted by N_A^m. For clarity, n and m are kept distinct even though they have to be equal. In matrix form,

$$\boldsymbol{N}\boldsymbol{q} = \boldsymbol{x} \tag{14}$$

Taking advantage of the isoparametric nature of *isogeometric* analysis, the same $\boldsymbol{N}$ matrix is applicable for the generalized displacements $\boldsymbol{u}^{\boldsymbol{q}} = \boldsymbol{q}(t) - \boldsymbol{q}(0)$,

$$\boldsymbol{N}\boldsymbol{u}^{\boldsymbol{q}} = \boldsymbol{u} \tag{15}$$

Using Equation (12) for all the interpolating points (and denoting $\boldsymbol{u}_{K_1}^{\infty}(\boldsymbol{x})$ the $2 \times n$ vector containing for each point the value of the asymptotic field),

$$\boldsymbol{u}_d = K_1 \boldsymbol{u}_{K_1}^{\infty}(\boldsymbol{x}) \tag{16}$$

The control point displacements are determined by introducing Equation (17) as a system of constraint equation during the analysis.

$$\boldsymbol{N}\boldsymbol{u}^{\boldsymbol{q}} - \boldsymbol{u}_d = 0 \tag{17}$$

Ideally, the system $\boldsymbol{N}$ is invertible, i.e. the correct number of interpolating points has to be chosen (the same as the number of unknowns including the enrichment functions that are non-zero on the boundary) and they have to be adequately distributed.

This method has been tested for some particular cases (the FE case and the case for a multiplicity of 1 on the interior knots values) and gives good results. An optimal convergence rate (equal to $p+1$ in the L_2 norm given by Equation (18)) for imposition of the displacement boundary condition has been verified for this method as shown in Figures 4(a) and (b);

$$e_{L_2} = \frac{\|\boldsymbol{u} - \boldsymbol{u}_{ex}\|_{L_2}}{\|\boldsymbol{u}_{ex}\|_{L_2}} \tag{18}$$

Figure 5 illustrate the method used to pick the correct number of constraints (some equivalent patterns can be found using Greville abscissae [26, 27]). In the presence of a Heaviside enrichment (see in Section 3), the number of interpolation points is doubled locally. Generalizing this approach for all possible multiplicities in the knot vectors and the presence of the enrichment functions is difficult, if we want to test a wide range of enrichment techniques.

2.3.2. Least-squares minimization. Instead of attempting to strongly impose the constraints on the control points via the exact number of required interpolating points on the boundary, the least-squares method naturally introduces a corresponding weak form. The least-squares error function J for a set of interpolating points on the boundary of the domain $\{\boldsymbol{x}^m, m \in \mathscr{M}\}$, where $\mathscr{M}$ is the set of points is

$$J = \frac{1}{2} \sum_{m \in \mathscr{M}} \left\| \sum_{A \in \mathscr{A}^m} N_A(s^m) \boldsymbol{q}_A - \boldsymbol{u}_d(\boldsymbol{x}^m) \right\|^2 \tag{19}$$

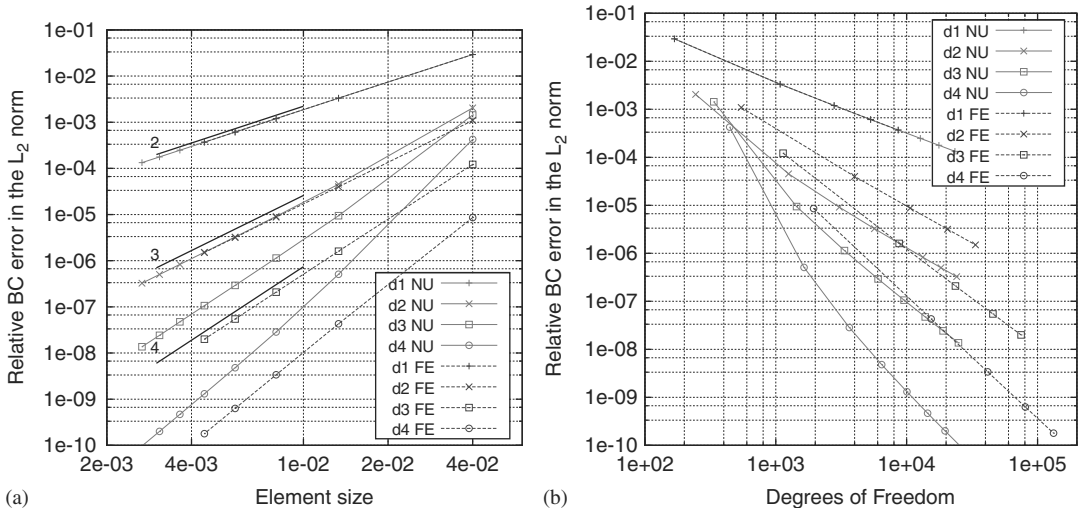

Figure 4. Error in the L_2 norm on the displacements imposed at the boundary, using the interpolating points method, for FE and NURBS. (a) Interpolating points method (element size) and (b) interpolating points method (DOF).

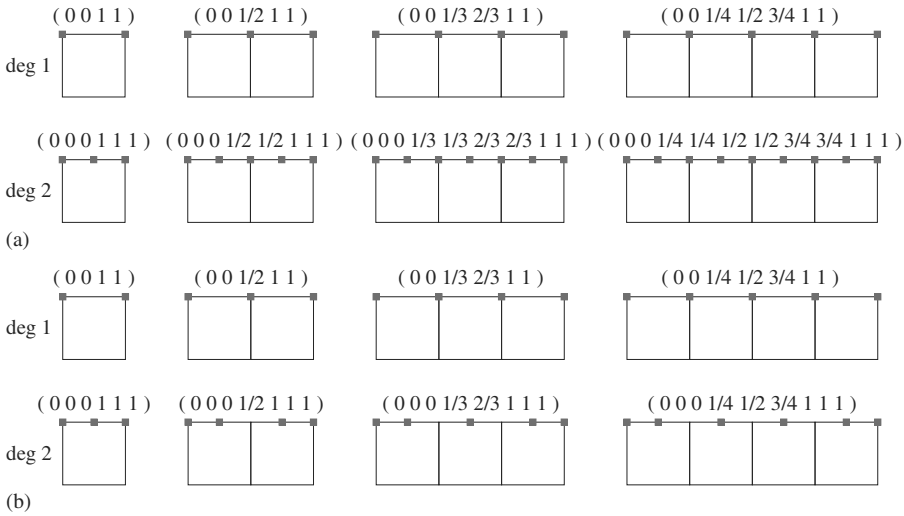

Figure 5. Location of the interpolating points for the linear constraints; degree 1 and 2, FE and NURBS. (a) Location for FE case and (b) location for NURBS case.

where $\mathscr{A}^m$ represents the indices of basis functions that are non-zero for the mth interpolation point. Minimizing J gives the linear system

$$\frac{\partial J}{\partial \boldsymbol{q}_B} = \sum_{m \in \mathscr{M}} \left(\sum_{A \in \mathscr{A}^m} N_A(s^m) \boldsymbol{q}_A - \boldsymbol{u}_d(\boldsymbol{x}^m) \right) N_B(s^m) = 0 \quad \forall B \in \mathscr{A} = \{ \cup \mathscr{A}^m, m \in \mathscr{M} \}. \tag{20}$$

Or equivalently,

$$\sum_{m \in \mathscr{M}} \sum_{A \in \mathscr{A}^m} N_B(s^m) N_A(s^m) \boldsymbol{q}_A = \sum_{m \in \mathscr{M}} \boldsymbol{u}_d(\boldsymbol{s}^m) N_B(s^m) \quad \forall B \in \mathscr{A} \tag{21}$$

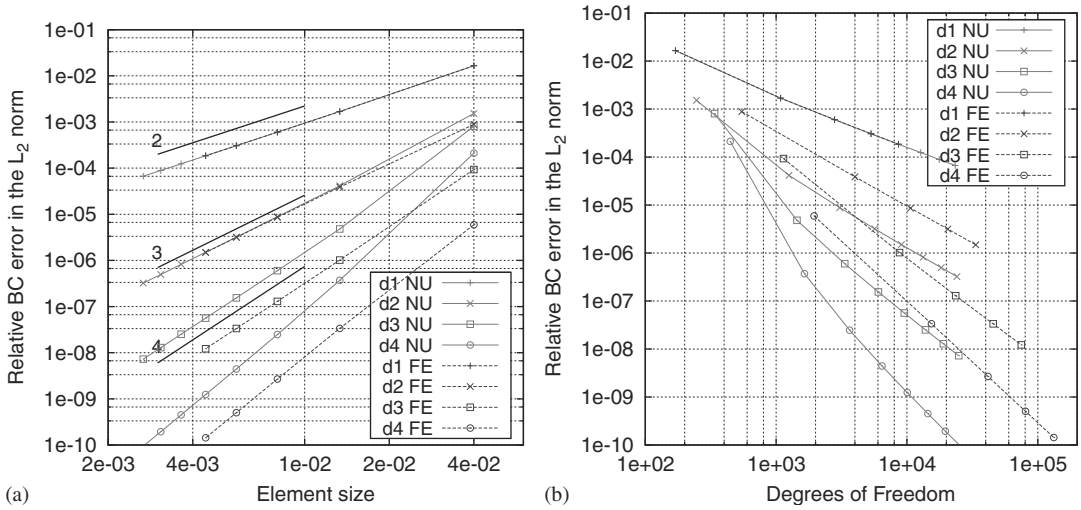

Figure 6. Error in the L_2 norm on the displacements imposed at the boundary, using a least-square minimization, for FE and NURBS. (a) Least-square minimization method (element size) and (b) least-square minimization method (DOF).

Re-numbering N and $\boldsymbol{q}$, Equation (21) becomes in a matrix form:

$$\sum_{m\in\mathscr{M}} \begin{pmatrix} N_1^m N_1^m & \dots & N_1^m N_n^m \\ \vdots & \ddots & \vdots \\ N_n^m N_1^m & \dots & N_n^m N_n^m \end{pmatrix} \begin{pmatrix} q_x^1 & q_y^1 & q_z^1 \\ \vdots & \vdots & \vdots \\ q_x^n & q_y^n & q_z^n \end{pmatrix} = \sum_{m\in\mathscr{M}} \begin{pmatrix} u_x^m N_1^m & u_y^m N_1^m & u_z^m N_1^m \\ \vdots & \vdots & \vdots \\ u_x^m N_n^m & u_y^m N_n^m & u_z^m N_n^m \end{pmatrix} \tag{22}$$

In the previous equation, n equals card($\mathscr{A}$), the total number of basis functions involved in the boundary displacements. Most of the basis functions N are actually null because of the local support of the basis functions. Enough points have to be taken for the system to be invertible. A direct solver for symmetric definite matrices is used to compute the control points displacements $\boldsymbol{q}_A$. Verification of the optimal convergence rate of $p+1$ in the L_2 norm on the displacements for the Dirichlet boundary condition problem is illustrated in Figures 6(a) and (b) for FE and NURBS for $p=1$ through $p=4$.

A sensitivity study regarding the number of interpolation points has been performed. Accuracy increases with the number of points until it equals the number of unknowns and then remains constant. Regarding the tip-enrichment strategy described in Section 4, the tip enrichment must not be active on the boundaries to avoid constraining the tip-enrichment DOF. For all practical purposes, using $2\times(p+1)$ points on each element edge on the boundary of the domain for basis functions of degree p is sufficient to determine all the unknowns. The case needing the highest number of equations is for a single enriched element; $p+1$ points are needed corresponding to the number of classical shape functions and $p+1$ additional ones for the Heaviside enrichments. This method is more flexible than the strong imposition method through the interpolating points constraints in the sense that a given number of evaluation points can be determined for a given degree of shape functions regardless of the particular multiplicities in the knot vector and specially regardless of whether an element is enriched or not.

The NURBS are slightly less efficient in term of the element size (see Figures 4(a) and 6(a)) but in terms of DOF, they are much more efficient (see Figures 4(b) and 6(b)). This difference in performance occurs for many of the comparisons in the remainder of this paper: based on the element size, FE appears superior, but based on the DOF, isogeometric analysis is superior. This difference stems from isogeometric analysis having a lower number of DOF per element than FE. Note that the cost of the analysis for implicit calculations is mainly due to the linear algebra which is a function of the band with and the number of equations in the stiffness matrix. Both

these values are function of the number of DOF; hence, decreasing the number of DOF decreases the computational cost. Note also that fewer DOF allows the use of fewer integration points [13] reducing the cost of explicit dynamic analysis.

3. STRONGLY DISCONTINUOUS ENRICHMENT AND CRACK COMPATIBILITY

3.1. Hansbo basis

Consider a 1D domain cut into two independent subdomains at $x=0.45$ as shown in Figure 7. To compute without any loss of accuracy in the two subdomains, two sets of basis functions are required with independent variables for the left and the right subdomains. Each cut basis function needs two independent control points: one for the left side and one for the right side. In one dimension this duplication introduces one additional DOF for each cut basis function. This choice of duplicating the basis function on either side of the cut is referred to as the Hansbo basis [28]. Using the Heaviside function H, defined in Equation (23), and its complement, denoted $\overline{H}$,

$$H(\boldsymbol{s})=\begin{cases}1 & \text{if } \boldsymbol{s} \text{ is on the right side of the crack}\\ 0 & \text{if } \boldsymbol{s} \text{ is on the left side}\end{cases} \tag{23}$$

$$\overline{H}(\boldsymbol{s})=1-H(\boldsymbol{s}) \tag{24}$$

the Hansbo basis may be formally expressed as:

$$\boldsymbol{x}(\boldsymbol{s},t)=\sum_{A\in\mathcal{N}} N_A(\boldsymbol{s})(\overline{H}(\boldsymbol{s})\overline{\boldsymbol{q}}_A(t)+H(\boldsymbol{s})\boldsymbol{q}_A(t)) \tag{25}$$

3.2. Heaviside enrichment

The *modified Heaviside* function H is defined as:

$$H(\boldsymbol{s})=\begin{cases}+1 & \text{if } \boldsymbol{s} \text{ is on one side of the crack}\\ -1 & \text{if } \boldsymbol{s} \text{ is on the other side}\end{cases} \tag{26}$$

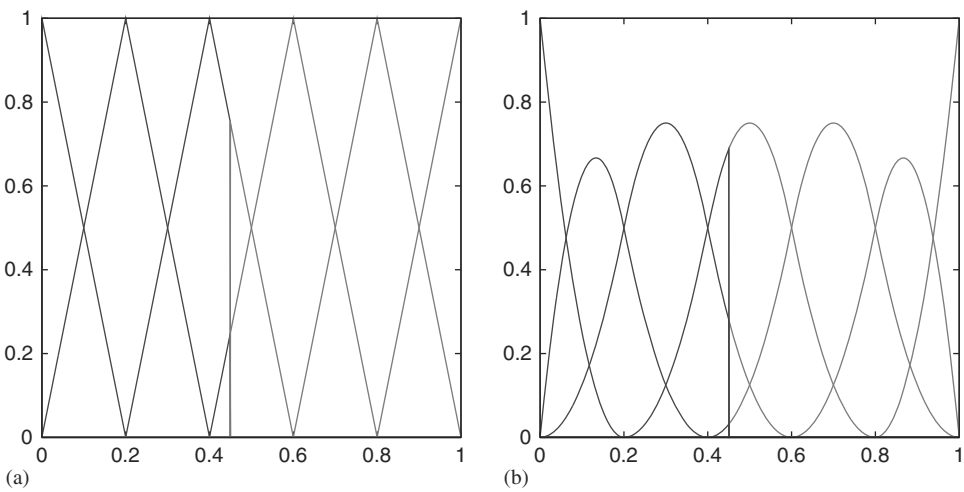

Figure 7. Hansbo basis functions in one dimension for 5 linear finite elements and 5 quadratic NURBS cut at $x=0.45$. (a) Hansbo basis for linear basis functions and (b) Hansbo basis for quadratic NURBS basis functions.

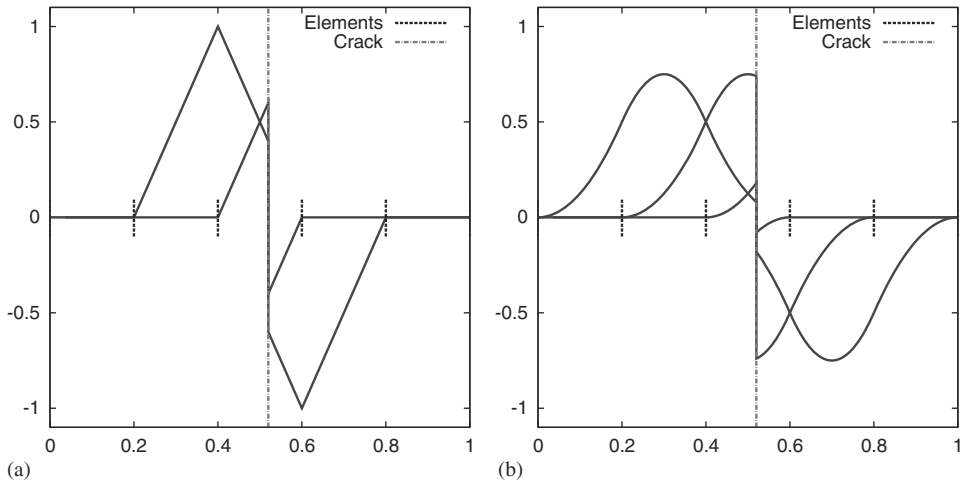

Figure 8. Enriched basis functions for (a) 5 linear finite elements and (b) 5 quadratic NURBS cut at $x = 0.45$.

A solution equivalent to the Hansbo basis is generated by augmenting the continuous basis functions $\{N_A\}$ (Figure 1) by the independent discontinuous vectors HN_A (Figure 8). The HN_A are independent from $\{N_A\}$ if they are cut by the discontinuity. The X-FEM approximation with NURBS basis functions is given by Equation (27) for the Heaviside enrichment:

$$\boldsymbol{u} = \sum_{A \in \mathscr{N}} N_A(s)\boldsymbol{q}_A + H(\boldsymbol{s}) \sum_{A' \in \mathscr{H}} \widetilde{N}_{A'}(s)\widetilde{q}_{A'} \tag{27}$$

Two options have been investigated for $\widetilde{N}$, the partition of unity used as a support for the enrichment functions:

- Use linear basis functions compatible with the NURBS elements,
- Use the basis functions N used in the classical part of the solution.

$\mathscr{H}$ contains the indices of every basis function belonging to the elements cut or partially cut by the discontinuity. With this enrichment technique, the basis functions whose index is in $\mathscr{H}$ build a partition of unity on the cut elements and a natural blending from the compact support of the basis functions (Figures 8 and 9). The support of the enrichment, $\sum \widetilde{N}_{A'}$ for A' in $\mathscr{H}$, is shown in Figure 9 with a dashed line. It is equal to 1 on the element cut by the crack (x from 0.4 to 0.6) where the partition of unity is realized, it transitions from 1 to 0 in the *blending* elements, and it remains 0 outside the blending elements. Depending on the degree of the basis functions, and on the multiplicity of the knot values in the knot vector, this blending layer can span several elements (two in the case of quadratic NURBS with a multiplicity equal to 1, as shown in Figure 9(b)).

The proposed X-FEM formulation was tested with a strong discontinuity for enrichment using the model linear fracture problem. One difficulty with this test is localizing the tip position. With standard FE, the last element is only partially enriched with the heaviside enrichment (two nodes of four for linear elements in 2-D) forcing the crack to end on the un-enriched side. In one formulation [29], the elements are continuously cut in order to smoothly propagate a crack using only Heaviside enrichments. For NURBS, the basis functions can span several elements. The position of the tip is controlled by using a weighting function for the Heaviside enrichment, denoted $B_{\mathscr{H}}$ in Equation (28) as shown in Figure 10. The resulting $B_{\mathscr{H}} H \sum N$ is represented in Figure 11; this enrichment technique allows handling the discontinuity introduced by the crack as well as ensuring an accurate position of the tip.

$$\boldsymbol{u} = \sum_{A \in \mathscr{N}} N_A(s)\boldsymbol{q}_A + B_{\mathscr{H}} H(\boldsymbol{s}) \sum_{A' \in \mathscr{H}} \widetilde{N}_{A'}(s)\widetilde{q}_{A'} \tag{28}$$

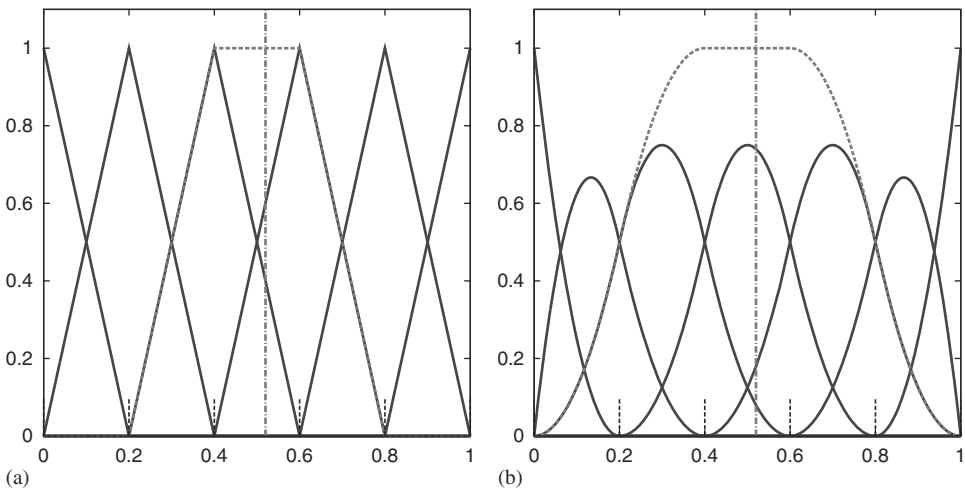

Figure 9. Enriched domain for 5 elements cut at $x = 0.45$. (a) Linear basis functions and (b) quadratic NURBS basis functions.

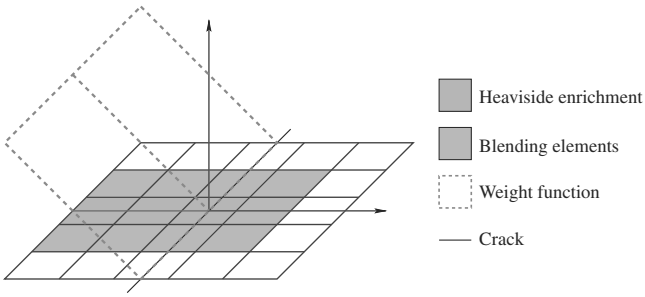

Figure 10. Enriched areas and weight function $B_{\mathscr{H}}$ used to localize the tip for FE and NURBS with the Heaviside enrichment only.

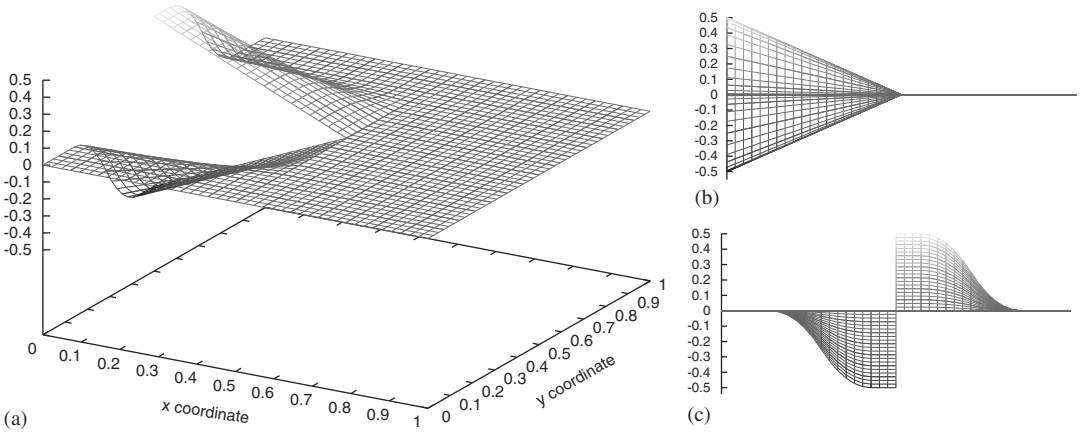

Figure 11. Heaviside enrichment for degree 2 NURBS weighted with the ramp function: $B_{\mathscr{H}} H \sum N$. (a) Perspective view; (b) X–Z projection: blending due to $B_{\mathscr{H}}$; and (c) Y–Z projection: blending due to $\sum N$.

This is an application of *blending*, a technique that will be discussed in detail in Section 4.2.1. A convergence study with only the Heaviside enrichment shows convergence for FE and NURBS only if the support for the Heaviside function is the same as the one used for the classical solution,

i.e. $\widetilde{N}=N$. With FE, for linear $\widetilde{N}$, the solution converges, but increasing the degree of N does not improve the solution (Figure 12(b)). With NURBS, linear $\widetilde{N}$ produces a slow divergence. This is illustrated in Figure 12 for NURBS and FE with $p=3$ for the classical solution, and a linear $\widetilde{N}$ for the Heaviside enrichment (Figures 12(a) and (b)) and for the same basis functions for both the classical part and the Heaviside enrichment (Figures 12(c) and (d)). The discontinuity on the ϵ_{yy} in Figure 12(a) is obvious, and it prevents the NURBS from converging. The reason for the lack of convergence will be discussed in detail in Section 4.3, but in brief, the presence of the C^0 lines between each element allows the classical continuous part of the solution to accommodate the discontinuity in the displacement introduced with the enrichment. Although increasing the degree improves the results in Figure 12(d), the convergence rate on the H_1 norm (Equation (29)) is limited to 0.5 because of the singular characteristic of the problem:

$$e_{H_1}=\frac{\|\boldsymbol{u}-\boldsymbol{u}_{ex}\|_{H_1}}{\|\boldsymbol{u}_{ex}\|_{H_1}} \tag{29}$$

3.3. Element integration

The integration is performed using Gauss quadrature. This method is efficient for polynomial functions and k integration points integrate exactly polynomial of degree $(2\times k-1)$ in one dimension, but it gives poor accuracy for discontinuous fields. To overcome this issue, the elements containing the discontinuity are subdivided as illustrated in Figure 13(b). The classical Gauss quadrature also gives poor accuracy for the singular enrichment used near the tip (in Section 4). The best results were obtained by using *almost polar integration* [21] for the element containing the crack tip enrichment. This integration method splits the quadrilaterals into triangles to concentrate the Gauss points near the tip as illustrated in Figure 13(c), giving a regular distribution of the integration points in terms of radius and angle (the polar coordinates relative to the tip). Figure 14 illustrates the integration efficiency for degree 3 and degree 4 NURBS shape functions enriched with the asymptotic field. Some optimal results have shown that very few integration points are needed to integrate NURBS shape functions [30]: half the number of shape functions is an indicative value for how many integration points are needed regardless of the degree of approximation. However, the presence of enrichments can highly penalize the integration efficiency. In our case, satisfactory accuracy has been reached with 5^2 integration points with the almost polar integration for degree 3 NURBS while the basic method hardly converges with 20^2 integration points (Figure 14(a)). With degree 4 NURBS, 16^2 integration points are needed with the almost polar integration in order to achieve convergence while the basic method does not guarantee enough precision (Figure 14(b)). This big increase is due to our particular problem where degree 4 NURBS perform really well; the integration error dominates in that case, and the integration effort is required to evaluate the convergence of the method in the presence of the tip enrichment. The 16^2 integration points will be used in the remainder for degree 4 shape functions, and for degree p shape functions when p is lower than 4, $(2\times p)^2$ integration points are used.

4. TIP ENRICHMENT

4.1. Combined Heaviside and singular crack tip enrichment

The convergence rate is limited with the Heaviside enrichment because of the singularity near the crack tip. For improved accuracy, the theoretical asymptotic field in mode I, given by Equation (11), is introduced into the solution space. The enrichment strategy in Equation (30) is based on X-FEM for higher order FEs [31, 32].

$$\boldsymbol{u}=\sum_{A\in\mathcal{N}}N_A\boldsymbol{q}_A+H(\boldsymbol{s})\sum_{A'\in\mathcal{H}}N_{A'}\widetilde{q}_{A'}+\boldsymbol{u}^{\infty}_{K_1}(\boldsymbol{s})\bar{q}\sum_{A''\in\mathcal{T}}N_{A''} \tag{30}$$

Only one additional DOF $\bar{q}$ is introduced to enrich the solution close to the tip with the theoretical asymptotic field. $\mathcal{T}$ contains the indices of every basis function used for the support of the tip

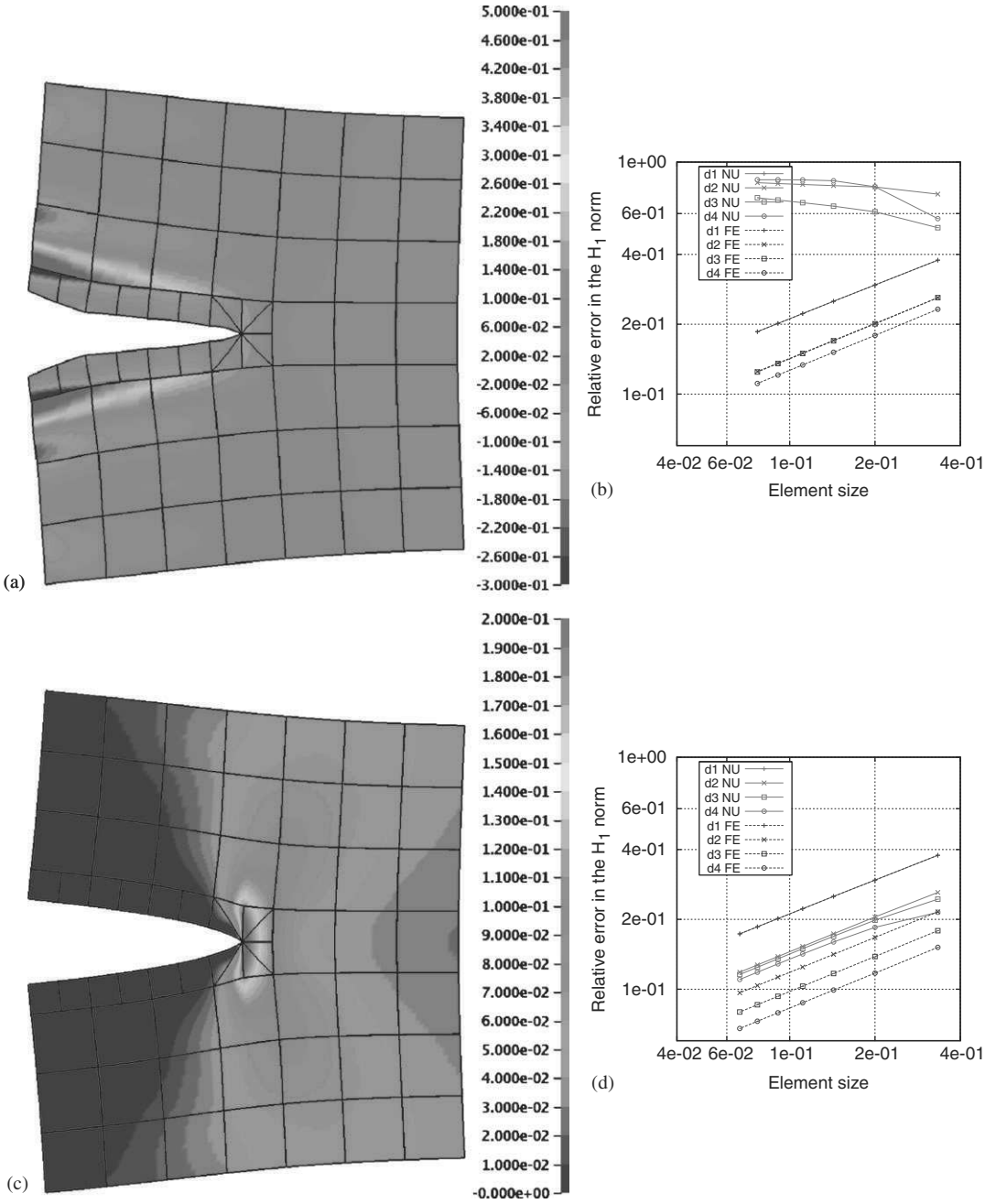

Figure 12. Influence of the Heaviside enrichment support: ϵ_{yy} strain component for 7×7 element with cubic NURBS basis functions and the Heaviside enrichment (element and sub-elements for integration are plotted; see in Section 3.3 for definitions), and convergence results. (a) ϵ_{yy} for NURBS shape functions for the classical part and a linear support for the Heaviside enrichment; (b) convergence with FE and linear $\widetilde{N}$ for the Heaviside enrichment but divergence for the NURBS; (c) ϵ_{yy} for NURBS shape functions for the classical part and the support of the Heaviside enrichment; and (d) convergence when the basis functions for the enrichment and the continuous part are the same.

enrichment. The singular enrichment function is not completely orthogonal to the NURBS basis functions, and therefore the contribution of the NURBS basis functions to the displacement field is not exactly zero even when the boundary displacement is driven by a pure mode I displacement field. As a consequence, the value of $\bar{q}$ does not exactly equal the stress-intensity factor K_1

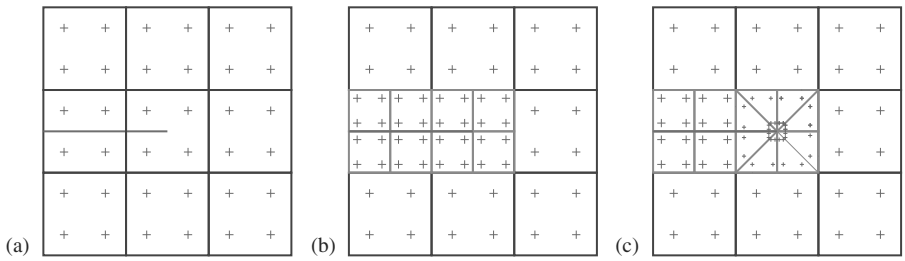

Figure 13. Integration strategy. (a) Initial; (a) sub-cells; and (c) almost polar.

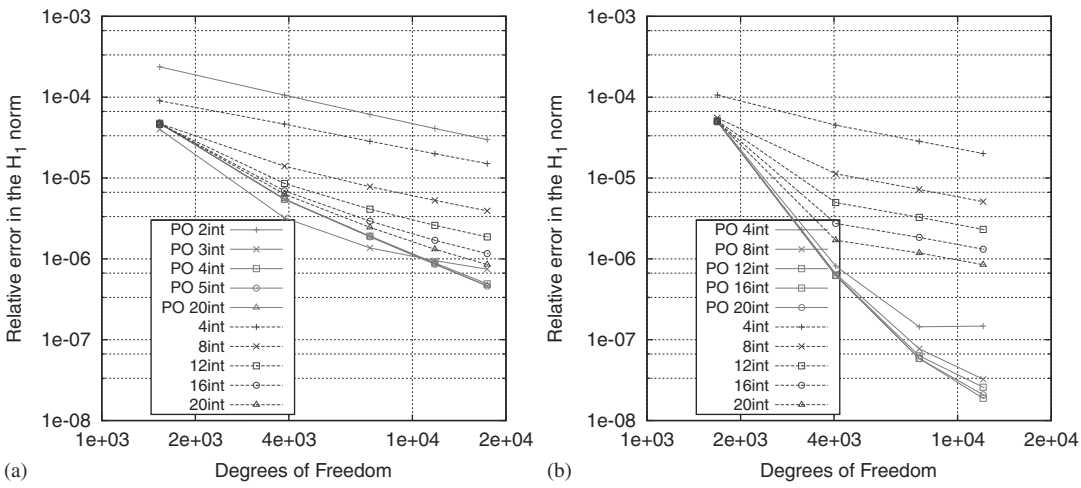

Figure 14. Integration efficiency: effect of the almost polar integration on the convergence. (a) Degree 3 NURBS shape functions and (b) degree 4 NURBS shape functions.

representing the total displacement field. The actual stress-intensity factor is found by minimizing $J(K_1)=\int_{\Omega_{\mathscr{T}}}(\boldsymbol{u}^h-\boldsymbol{u}^{\infty}_{K_1}K_1)^2\,\mathrm{d}\Omega$ where $\Omega_{\mathscr{T}}$ is a domain surrounding the tip. Approximating the integration with the Gauss quadrature, with $G_{\mathscr{T}}$ the Gauss points located in a neighborhood of the tip, introducing the integration weights w_g, and setting $\mathrm{d}J/\mathrm{d}K_1=0$, the expression for the value of K_1 based on the calculated displacement field is

$$K_1=\frac{\sum_{g\in G_{\mathscr{T}}} w_g\boldsymbol{u}^h(\boldsymbol{x}_g).\boldsymbol{u}^{\infty}_{K_1}(\boldsymbol{x}_g)}{\sum_{g\in G_{\mathscr{T}}} w_g\boldsymbol{u}^{\infty}_{K_1}(\boldsymbol{x}_g).\boldsymbol{u}^{\infty}_{K_1}(\boldsymbol{x}_g)} \tag{31}$$

The results in Table I show the convergence for both the mode I stress-intensity factor K_1 computed according to Equation (31) and the tip-related DOF. Nevertheless the first option leads to an improved error estimate due to the fact that the contribution of the continuous part and the Heaviside enrichment are not necessary equal to zero near the tip. In order to illustrate it, the contribution from the continuous part is plotted in Figure 15 for the different techniques investigated in the remainder. We can see that the total displacement is partitioned into the continuous part and the various enrichments even in the central part where the tip enrichment is present as the continuous contribution is not necessarily zero.

As pointed out in the previous section, the support for the enrichment functions is the same as the one used for the classical continuous contribution. The only set of basis functions remaining is the N_A where A is in $\mathscr{N}$ for the classical continuous part, in $\mathscr{H}$ for the Heaviside enrichments,

Table I. Error on the stress-intensity factor computed with Equation (31) and on the tip-related DOF denoted $\bar{q}$ Equation (30) for linear and cubic NURBS shape functions and C^0 lines as illustrated in Figure 21.

	Degree 1		Degree 3	
Element	Tip-related DOF	Computed K_1	Tip-related DOF	Computed K_1
5×5	6.08E−03	3.88E−03	8.55E−05	2.94E−05
25×25	3.50E−04	5.49E−04	2.76E−07	1.34E−07
45×45	1.36E−04	1.81E−04	3.26E−08	1.92E−09

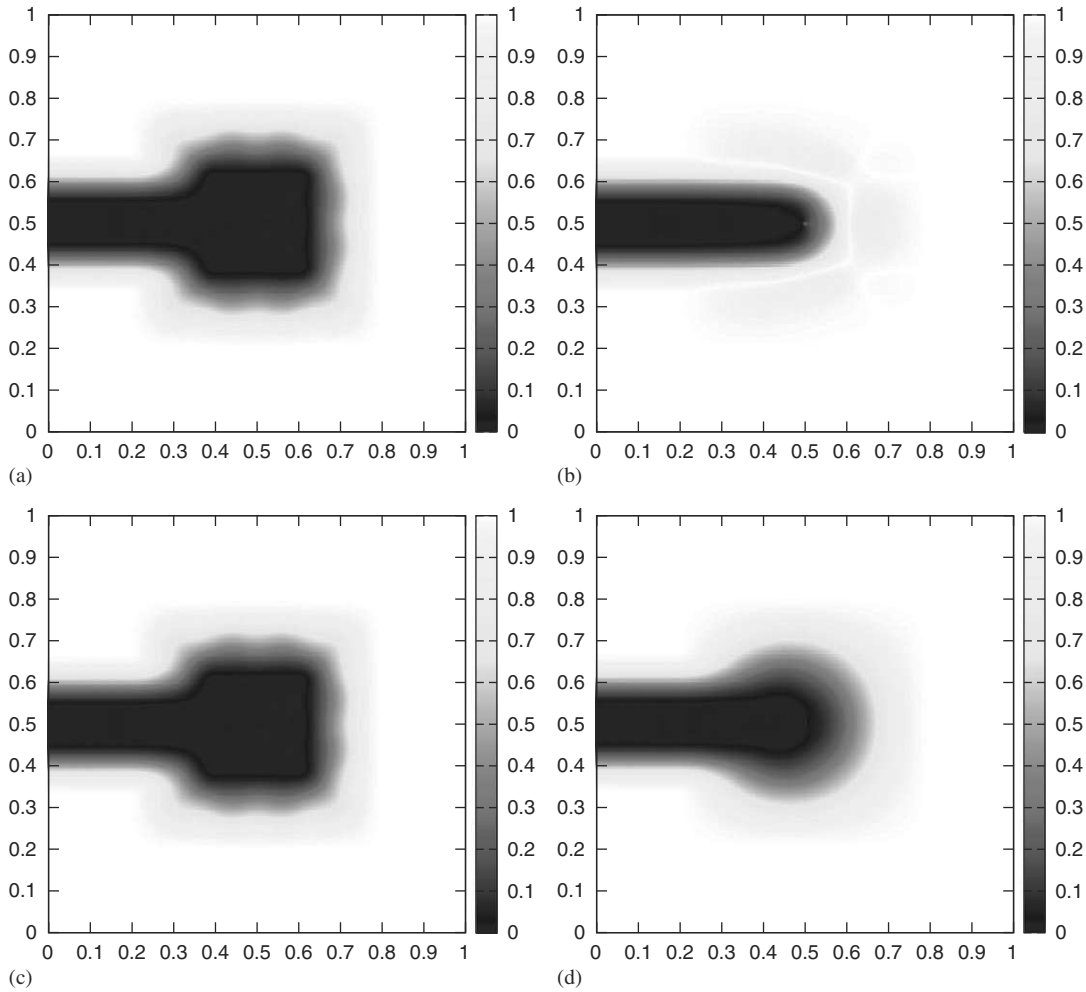

Figure 15. Norm of the contribution from the classical continuous part of the displacement relative to the norm of the total displacement for a mesh of 15×15 elements with quadratic NURBS. (a) One DOF for the tip enrichment; (b) one DOF for each shape function involved in the support of the tip enrichment; (c) one DOF for the tip enrichment and projected blending; and (d) one DOF for each shape function involved in the support of the tip enrichment and projected blending.

and in $\mathscr{T}$ for the tip enrichments. The subdomains enriched with the crack tip asymptotic solution and the Heaviside function, and the corresponding blending subdomains are shown in Figure 16. The fully enriched subdomains are the ones where the support of the enrichment functions fulfills a partition of unity. The blending subdomains incorporate a transition to ensure compatibility between the two enrichment functions and with the un-enriched domain.

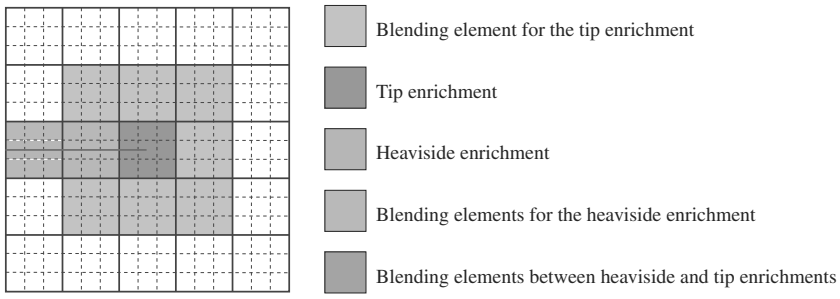

Figure 16. Heaviside plus tip enrichment subdomains.

4.2. *Compatibility enforcement*

Compatibility has to be enforced at the boundaries of the enriched subdomains. Two techniques are commonly used:

- *Blending*: Multiply the enrichment function by a bubble function so that it goes to zero on the boundaries of the enriched subdomain [33].
- *Shifting*: Subtract from the enrichment functions linear combinations of a subset of the N so that their value on the boundaries of the enriched subdomain will be zero [34].

4.2.1. Blending. Two different blending techniques are considered. The first one takes advantage of the evanescence of the basis functions. Compatibility between the two enrichment functions is enforced by removing the redundant basis function indices from $\mathscr{H}$ or $\mathscr{T}$ so that $\mathscr{H} \cap \mathscr{T} = \{\emptyset\}$. In practice, $\mathscr{T}$ is constructed by including every index of a basis function belonging to the subdomain where we want the tip enrichment to be active, as illustrated in Figure 9, then each index of a basis function cut by the crack that is not in $\mathscr{T}$ is added to $\mathscr{H}$ as illustrated in Figure 17(b). This technique is very simple and guarantees compatibility between the various subdomains. A convergence study revealed that the different subdomains vary in area according to the degree of mesh refinement, leading to suboptimal convergence rates. In Figure 18, the order of convergence is limited to 1 even with the higher degree basis functions. The explanation is that the blending area increases with the degree of the basis functions because NURBS of degree p span $p+1$ elements (see Figure 9 for an increasing order) but the area of the crack tip enrichment decreases as the mesh is refined (the support of the basis functions is reduced). This problem has been observed by others [32]. To circumvent it, the blending functions $B_{\mathscr{H}}$ for the Heaviside and $B_{\mathscr{T}}$ for the tip-enrichment functions are introduced [33, 32] (Figure 19).

$$\boldsymbol{u} = \sum_{A \in \mathscr{N}} N_A \boldsymbol{q}_A + B_{\mathscr{H}} H \sum_{A' \in \mathscr{H}} N_{A'} \widetilde{q}_{A'} + B_{\mathscr{T}} \boldsymbol{u}_{K_1}^{\infty} \bar{q} \sum_{A'' \in \mathscr{T}} N_{A''} \tag{32}$$

The region for the tip enrichment is therefore controlled by where the blending function $B_{\mathscr{T}}$ is nonzero (Figure 19) and made independent of the degree of the basis functions and the degree of mesh refinement. The blending function decreases with the distance from the crack tip to enforce compatibility with the unenriched subdomains. For the Heaviside enrichment, the strategy developed in Section 3 is used. The basis functions cut by the discontinuity are extracted and enriched. The compatibility with the unenriched area is guaranteed via the evanescence of the selected basis functions. To ensure the compatibility between the tip and the Heaviside enrichment functions, $B_{\mathscr{H}} + B_{\mathscr{T}} = 1$ around the crack tip subdomain and $B_{\mathscr{T}}$ decreases radially depending on the distance from the tip. $\mathscr{T}$ is therefore not used to define the region of the crack tip enrichment, and the $N_{A''}$ form a partition of unity on the whole support of $B_{\mathscr{T}}$. Equation (32) can therefore be simplified to

$$\boldsymbol{u} = \sum_{A \in \mathscr{N}} N_A \boldsymbol{q}_A + B_{\mathscr{H}} H \sum_{A' \in \mathscr{H}} N_{A'} \widetilde{q}_{A'} + B_{\mathscr{T}} \boldsymbol{u}_{K_1}^{\infty} \bar{q}. \tag{33}$$

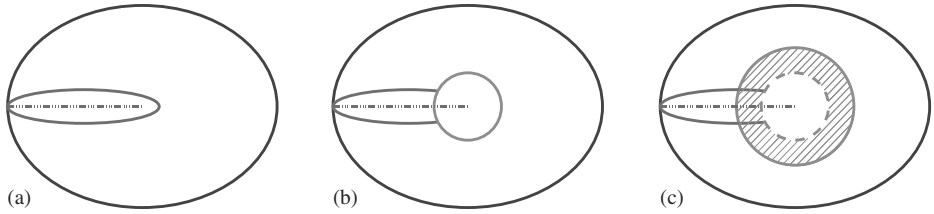

Figure 17. Heaviside $\mathscr{H}$, and tip $\mathscr{T}$, indices of enriched control points regarding the chosen blending technique. (a) Inclusion of $\mathscr{H}$, index of Heaviside-enriched control points, into $\mathscr{N}$; (b) $\mathscr{H} \cap \mathscr{T} = \{\emptyset\}$ blending by selection of the basis functions; and (c) $\mathscr{H} \cap \mathscr{T} \neq \{\emptyset\}$ with blending functions.

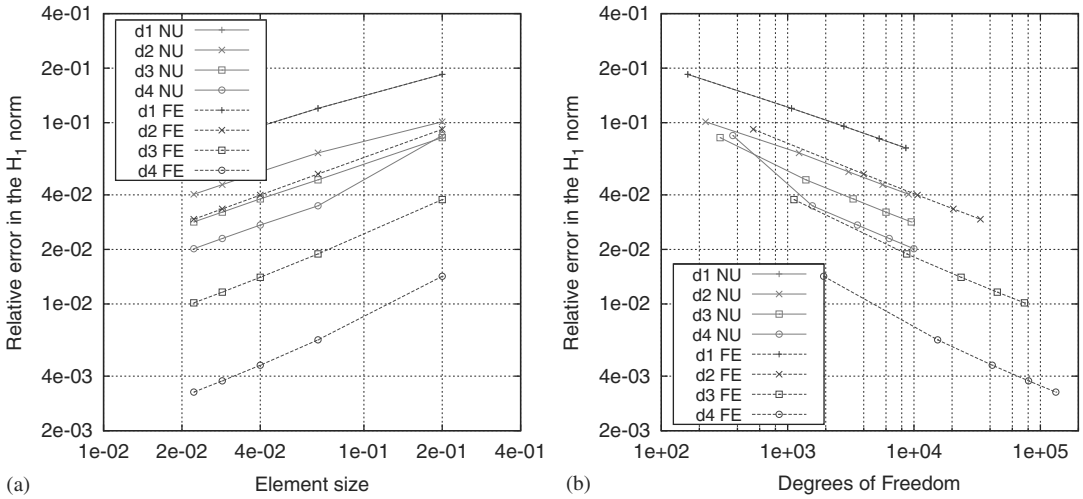

Figure 18. Convergence with blending by the selection of the basis functions and with no shifting.

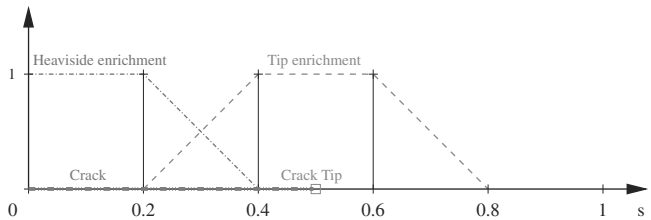

Figure 19. Linear blending functions for the Heaviside enrichment $B_{\mathscr{H}}$, and the tip enrichment $B_{\mathscr{T}}$.

For simplicity, the blending functions were chosen to be linear (bi-linear in two dimensions) as illustrated in Figure 19.

4.2.2. Shifting. The other option to enforce compatibility is to shift the enrichment functions as first described by Belytschko [34]. The shifted enrichment function is generated by subtracting a projection of the enrichment function on to the basis functions within the enriched subdomain from the enrichment function, thereby guaranteeing that the shifted enrichment function is zero on the boundary of the enriched subdomain.

$$\boldsymbol{u} = \sum_{A \in \mathscr{N}} N_A \boldsymbol{q}_A + B_{\mathscr{H}} \sum_{A' \in \mathscr{H}} (H - \beta_{A'}) N_{A'} \widetilde{q}_{A'} + B_{\mathscr{T}} \bar{q} \sum_{A'' \in \mathscr{T}} (\boldsymbol{u}_{K_1}^{\infty} - \boldsymbol{\beta}_{A''}) N_{A''} \tag{34}$$

For the standard FEM, the projection consists of the interpolant of the enrichment function. Taking advantage of the Kronecker-delta property, $\beta_{A'} = H(\boldsymbol{x}_{A'})$, the value of the Heaviside function at

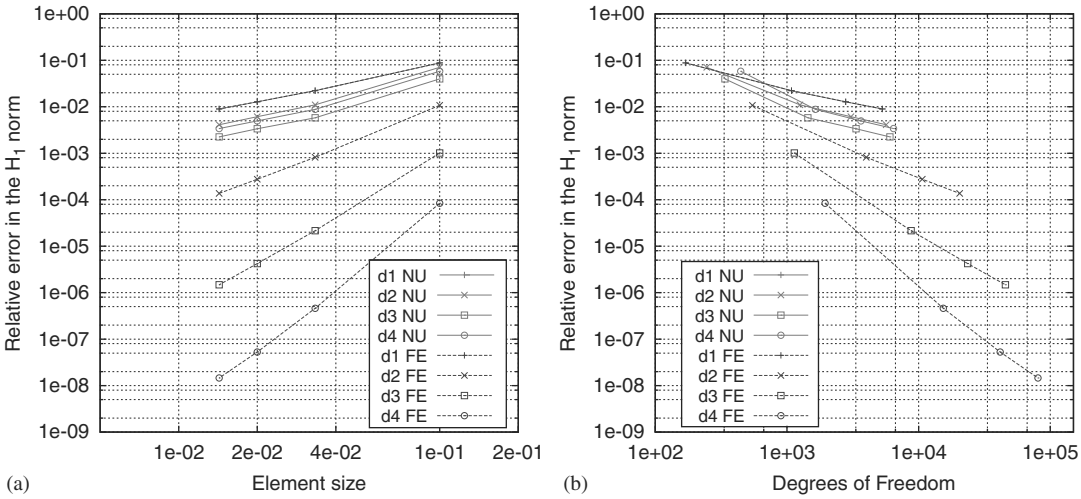

Figure 20. Convergence in the H_1 norm as a function of the element size and the number of DOF using Equation (33) with the blending function.

the *node* and $\boldsymbol{\beta}_{A''} = \boldsymbol{u}^{\infty}_{K_1}(\boldsymbol{x}_{A''})$, the value of the asymptotic crack tip field. For NURBS, using this technique with the control point instead of the node will be called *basic shifting*. This method for the Heaviside enrichment can be applied in a straight forward manner to NURBS because the Heaviside function is piecewise constant. Solving for the $\boldsymbol{\beta}_{A''}$ by minimizing $\|\boldsymbol{u}^{\infty}_{K_1} - \sum \boldsymbol{\beta}_{A''} N_{A''}\|$ via a least-squares minimization is referred to as *improved shifting*. This shifting technique is applied only to the tip enrichment using a single DOF.

4.3. Convergence study

The convergence of Equation (33), using the blending function illustrated in Figure 19 and without shifting, is shown in Figure 20. The NURBS basis functions do not converge or converge slowly. Optimal convergence is obtained when each knot has its multiplicity increased until the multiplicity is equal to the degree. This solution is denoted 'FE' because the continuity between the elements is only C^0 and the basis functions span the same space as the traditional Lagrangian basis functions of the same degree. This limitation is due to the 'incompatibility' of the degree of continuity between the basis functions and the blending functions for the NURBS. For example, the blending functions illustrated in Figure 19 are C^0 while the NURBS are C^{p-1}. This difference in continuity forces the kinks introduced by the enrichment functions to remain in the final solution as the NURBS cannot accommodate this C^1 discontinuity, and leads to poor convergence for the higher degree NURBS. This can be overcome in two ways:

- Add C^0 lines (Figure 21) to separate the enriched, unenriched, and blending subdomains.
- Introduce a blending function that is compatible with the higher order basis functions used in the classical part of the solution, and additional DOF for the tip enrichment, as in Equation (35).

4.3.1. C^0 lines. The first option to guarantee the compatibility of the blending functions with the classical approximation is to introduce C^0 lines along the slope discontinuities of the blending functions as illustrated in Figure 21. These C^0 lines are naturally present with the classical FE and permit the solution to accommodate the weak discontinuity introduced via the blending function. The C^0 lines are generated by raising the multiplicity of the corresponding knot values to equal the degree of the approximation. Figure 22 shows optimal convergence for both the NURBS and the FE case with this strategy. Unfortunately, this option imposes some constraints on the knot vector as a multiplicity equal to the degree should be found at the weak discontinuities of the blending function. This option is not flexible enough to use with arbitrary meshes. This operation is not

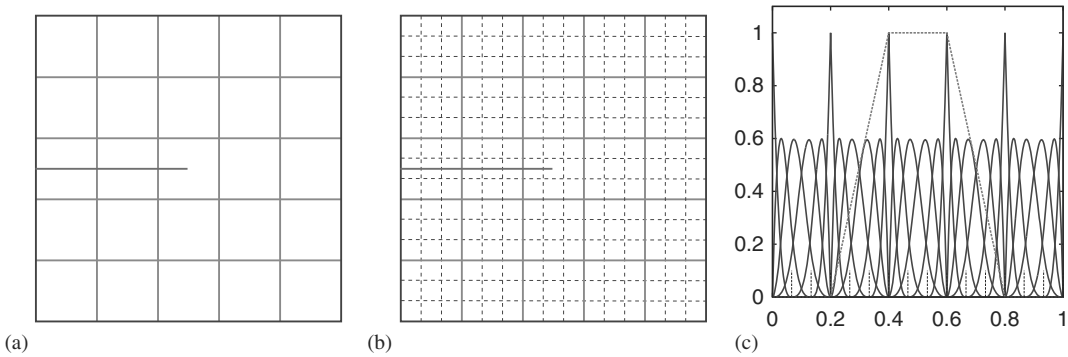

Figure 21. Mesh refinement with C^0 lines at $k = 0.2, 0.4, 0.6$ and 0.8, and corresponding 1D NURBS basis functions of degree 3. (a) Initial; (b) First refinement; (c) 1D basis functions.

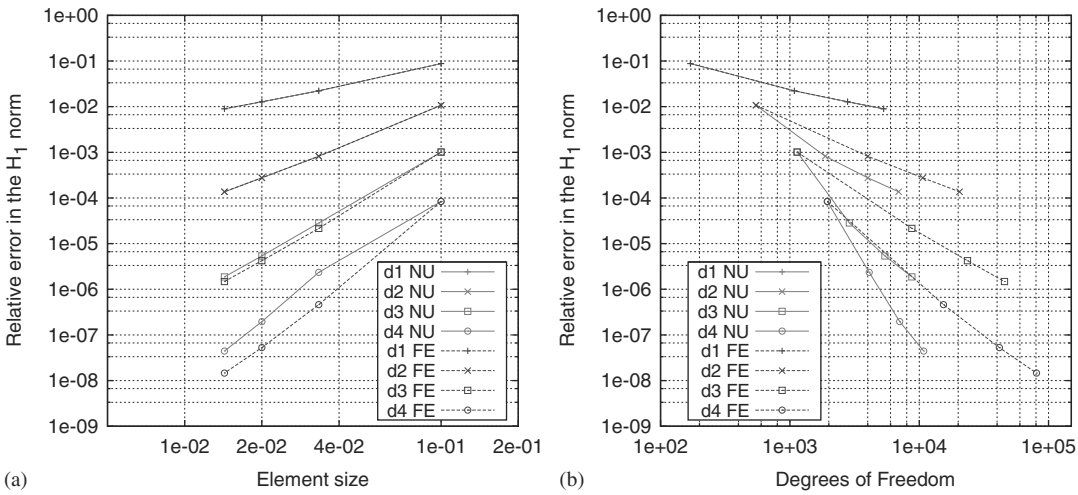

Figure 22. Convergence in the H_1 norm as a function of the element size and the number of DOF with C^0 lines compatible with the blending functions, formulation of Equation (33).

Table II. Order of convergence on the H_1 norm for an h-refinement with NURBS shape functions and C^0 lines as illustrated in Figure 21.

Degree	Without blending	With blending
1	1.00	1.00
2	2.02	2.09
3	3.13	3.49
4	4.51	5.26

Equation (34) is used with the improved shifting technique. In that case, the compatibility is already achieved, but some blending can still be used.

strictly a remeshing as the number of elements remains the same, but the basis functions and their number are changed. Nevertheless, this option improves the order of convergence for the NURBS from degree 1 to 4. The results are shown in Table II with some super-convergence evident for the higher degree NURBS.

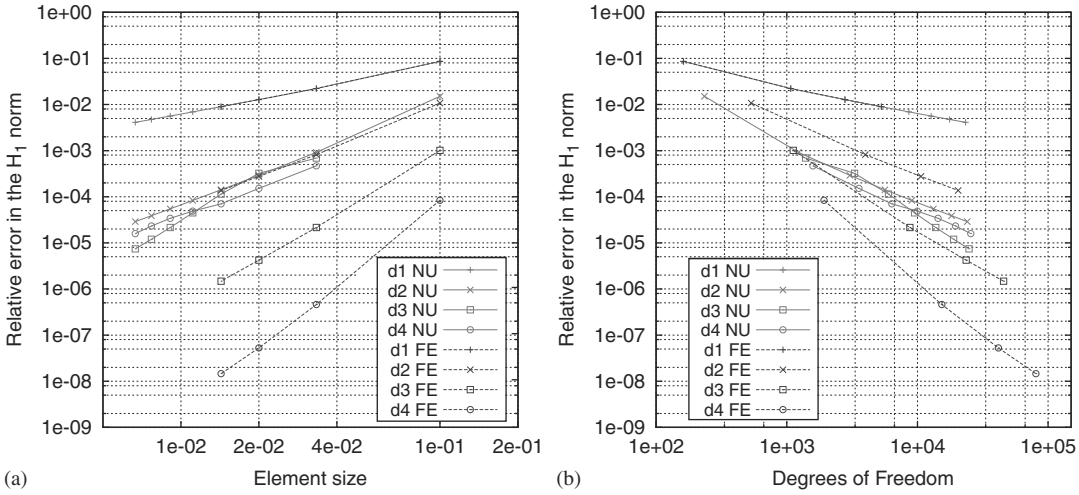

Figure 23. Convergence on the H_1 norm as a function of the element size and the number of DOF for the projected blending function formulation of Equation (35).

4.3.2. Projected blending function. Instead of using the blending functions introduced in Equations (32) and (33), the support for the enrichment functions is modified by projecting the blending function on the shape functions. The scalars $B^{\mathscr{H}}_{A'}$ and $B^{\mathscr{T}}_{A''}$ are as follows:

$$\boldsymbol{u} = \sum_{A\in\mathscr{N}} N_A \boldsymbol{q}_A + H \sum_{A'\in\mathscr{H}} B^{\mathscr{H}}_{A'} N_{A'} \tilde{q}_{A'} + \boldsymbol{u}^{\infty}_{K_1} \bar{q} \sum_{A''\in\mathscr{T}} B^{\mathscr{T}}_{A''} N_{A''} \tag{35}$$

These constants are calculated so that $\sum B^{\mathscr{H}}_{A'} N_{A'}$ and $\sum B^{\mathscr{T}}_{A''} N_{A''}$ match as closely as possible the previous blending functions $B_{\mathscr{H}}$ and $B_{\mathscr{T}}$ (illustrated in Figure 19). The $B^{\mathscr{T}}_{A''}$ are determined by first setting them to 0 for the basis functions spanning the unenriched domain, to 1 over the fully enriched domain, and the remaining values are obtained from a least-squares minimization for the basis functions spanning only the blending domain. The $B^{\mathscr{H}}_{A'}$ are then calculated so that $B^{\mathscr{H}}_{A} + B^{\mathscr{T}}_{A} = 1$ on the blending domain between the tip and the Heaviside-enrichment functions. This formulation, illustrated in Figure 23, performs better than the one with the weakly discontinuous blending functions in Equations (32) and (33).

Additional accuracy is obtained for the formulations given by Equations (32) and (33) when an additional DOF is introduced for each enriched basis function in Equation (36) as shown in Figure 24.

$$\boldsymbol{u} = \sum_{A\in\mathscr{N}} N_A \boldsymbol{q}_A + B_{\mathscr{H}} H \sum_{A'\in\mathscr{H}} N_{A'} \tilde{q}_{A'} + B_{\mathscr{T}} \boldsymbol{u}^{\infty}_{K_1} \sum_{A''\in\mathscr{T}} N_{A''} \bar{q}_{A''} \tag{36}$$

Even better convergence, however, is obtained when using the projected blending function and introducing an additional DOF for each enriched basis function in Equation (37) as shown in Figure 25:

$$\boldsymbol{u} = \sum_{A\in\mathscr{N}} N_A \boldsymbol{q}_A + H \sum_{A'\in\mathscr{H}} B^{\mathscr{H}}_{A'} N_{A'} \tilde{q}_{A'} + \boldsymbol{u}^{\infty}_{K_1} \sum_{A''\in\mathscr{T}} B^{\mathscr{T}}_{A''} N_{A''} \bar{q}_{A''} \tag{37}$$

5. CONCLUSION

The combination of isogeometric analysis with X-FEM produces high levels of accuracy with optimal convergence rates for linear fracture mechanics. The most convenient method for imposing Dirichlet boundary conditions was found to be a least-squares procedure. Several options for

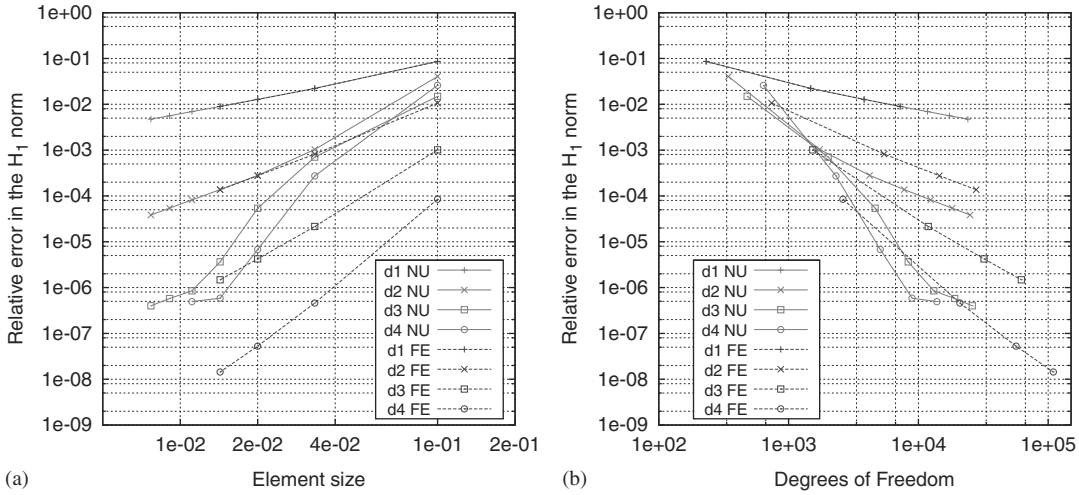

Figure 24. Convergence on the H_1 norm as a function of the element size and the number of DOF for formulation of Equation (36), where there is an additional DOF for each tip-enriched shape function.

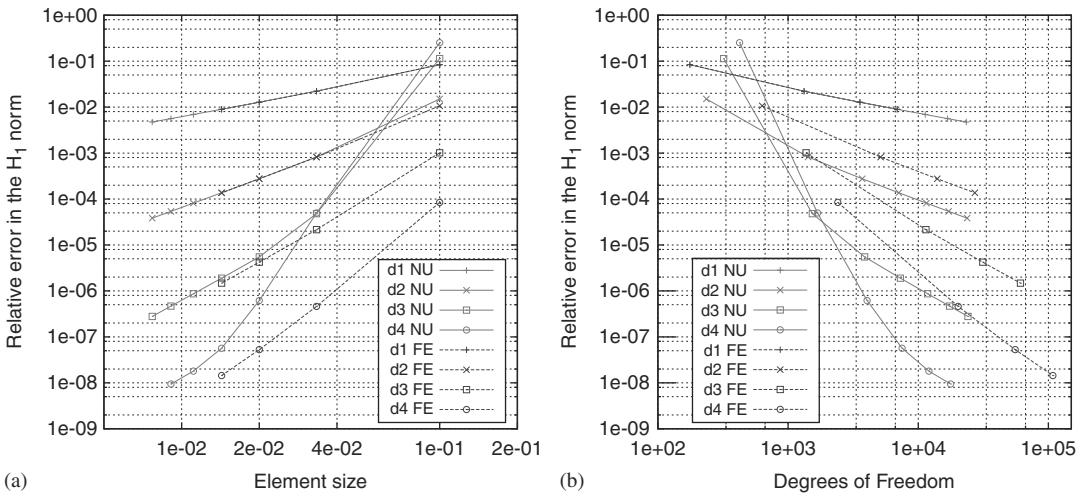

Figure 25. Convergence on the H_1 norm as a function of the element size and the number of DOF for the projected blending function and an additional DOF for each tip-enriched shape function, Equation (37).

blending and shifting the enrichment function are proposed, and the convergence rates were found to be very sensitive to them. The best solutions were obtained by using a modified projection method to generate the blending functions and independent degrees of freedom for each basis function $N_{A''}$ in the crack tip-enrichment subdomain. The full potential of the method should be revealed when dealing with complex geometries as well as curved cracks. Indeed, NURBS offers the possibility for describing exactly a given geometry regardless of the mesh coarseness. The primary difficulty with curved cracks is the integration of the cut elements requires some special treatment. One way of dealing with this complexity is the NURBS-enhanced FEM [35]. This will be explored in a future paper.

APPENDIX A: IMPLEMENTATION USING GENERALIZED ELEMENTS

The isogeometric X-FEM was implemented using the *generalized element* formulation [13]. This option, available in LS-DYNA, permits the investigation of a broad range of X-FEM options

without any additional programming. The formulation is briefly summarized here with an emphasis on how the anisotropic crack tip-enrichment functions are handled. For brevity and simplicity, the details associated with the blending and shifting functions are omitted.

A traditional isoparametric FE formulation is defined in terms of its parametric coordinate system $\boldsymbol{s}$, its basis functions $N_A(\boldsymbol{s})$ and their derivatives $\partial N_A/\partial \boldsymbol{s}$ for $A=1,n$, and a numerical integration rule over the element domain defined in terms of the locations of the integration points $\boldsymbol{s}^g$ and their weights w_g for $g=1,n_{gp}$ points. The numerical evaluation of the stiffness matrix and the residual only needs the numerical values of the basis functions and their derivatives at the integration points, i.e. their analytical form is never needed for numerical calculations. An element formulation may therefore be specified entirely through the input file containing the required values of w_g, $N_A(\boldsymbol{s}^g)$, and $\partial N_A(\boldsymbol{s}^g)/\partial \boldsymbol{s}$.

The kinematics of the generalized element have the standard form,

$$\boldsymbol{x}(\boldsymbol{s},t)=N_A(\boldsymbol{s})\boldsymbol{q}_A(t) \tag{A1}$$

where $\boldsymbol{q}(t)$ is a time dependent vector of generalized coordinates. This form leads to the usual definitions and forms for the Jacobian matrix $\boldsymbol{J}$ and the discrete gradient operator $\boldsymbol{B}$. The contribution of the stress to the internal force is therefore

$$\boldsymbol{F}=\int_V \boldsymbol{B}^{\mathrm{T}}\boldsymbol{\sigma}\,\mathrm{d}V=\sum_g \boldsymbol{B}^{\mathrm{T}}(\boldsymbol{s}^g)\boldsymbol{\sigma}(\boldsymbol{s}^g)w_g\det(\boldsymbol{J}) \tag{A2}$$

and differentiation of the internal force gives the stiffness matrix.

Equation (A1) requires that the dimension of $\boldsymbol{q}$ to be the same as the number of spatial dimensions and uses the same basis functions in each spatial direction, two conditions that are not met by the enrichment functions used for the crack tip. To incorporate them within the generalized element framework, two additional basis functions are introduced,

$$N_1^\infty=\sum_A N_A\frac{\sqrt{r}}{2\sqrt{2\pi}\mu}\left\{\left(-\frac{1}{2}+k\right)\cos\left(\frac{\theta}{2}\right)-\cos\left(\frac{3\theta}{2}\right)\right\} \tag{A3}$$

$$N_2^\infty=\sum_A N_A\frac{\sqrt{r}}{2\sqrt{2\pi}\mu}\left\{\left(+\frac{1}{2}+k\right)\sin\left(\frac{\theta}{2}\right)-\sin\left(\frac{3\theta}{2}\right)\right\} \tag{A4}$$

and the displacement field is enriched with a surplus of DOF,

$$\boldsymbol{u}_{K_1}^\infty=N_1^\infty\begin{Bmatrix}u_{11}^\infty\\u_{12}^\infty\\u_{13}^\infty\end{Bmatrix}+N_2^\infty\begin{Bmatrix}u_{21}^\infty\\u_{22}^\infty\\u_{23}^\infty\end{Bmatrix} \tag{A5}$$

The desired displacement field is

$$\boldsymbol{u}_{K_1}^\infty=N_1^\infty\begin{Bmatrix}K_1\\0\\0\end{Bmatrix}+N_2^\infty\begin{Bmatrix}0\\K_1\\0\end{Bmatrix} \tag{A6}$$

and it is obtained by equating the terms in Equations (A5) and (A6) to generate the constraint equations

$$u_{11}^\infty-u_{22}^\infty=0 \tag{A7}$$

$$u_{12}^\infty=0 \tag{A8}$$

$$u_{13}^\infty=0 \tag{A9}$$

$$u_{21}^\infty=0 \tag{A10}$$

$$u_{23}^\infty=0 \tag{A11}$$

Unlike most basis functions, the crack tip enrichment uses both the parametric coordinates $\boldsymbol{s}$ and the physical coordinates $\boldsymbol{x}$. The required derivatives are evaluated in the parametric coordinate system via the chain rule, e.g.

$$\frac{\partial N_A \boldsymbol{u}_{K_1}^{\infty}}{\partial \boldsymbol{s}} = \frac{\partial N_A}{\partial \boldsymbol{s}} \boldsymbol{u}_{K_1}^{\infty} + N_A \frac{\partial \boldsymbol{u}_{K_1}^{\infty}}{\partial \boldsymbol{x}} \cdot \frac{\partial \boldsymbol{x}}{\partial \boldsymbol{s}}. \tag{A12}$$

ACKNOWLEDGEMENTS

The support of the National Science Foundation under grant 07-00204 and the Office of Naval Research under grants N00014-08-1-1191 and N00014-10-1-0043 are gratefully acknowledged.

REFERENCES

1. Koh H, Lee H, Haber R. Dynamic crack propagation analysis using Eulerian–Lagrangian kinematic descriptions. *Computational Mechanics* 1988; **3**(3):141–155.
2. Swenson D, Ingraffea A. Modeling mixed-mode dynamic crack propagation nsing finite elements: theory and applications. *Computational Mechanics* 1988; **3**(6):381–397.
3. Belytschko T, Tabbara T. Dynamic fracture using element-free Galerkin methods. *International Journal for Numerical Methods in Engineering* 1996; **39**:923–938.
4. Fleming M, Chu Y, Moran B, Belytschko T. Enriched element-free Galerkin methods for crack tip fields. *International Journal for Numerical Methods in Engineering* 1997; **40**(8):1483–1504.
5. Bordas S, Rabczuk T, Zi G. Three-dimensional crack initiation, propagation, branching and junction in non-linear materials by an extended meshfree method without asymptotic enrichment. *Engineering Fracture Mechanics* 2008; **75**(5):943–960.
6. Belytschko T, Black T. Elastic crack growth in finite elements with minimal remeshing. *International Journal for Numerical Methods in Engineering* 1999; **45**(5):601–620.
7. Moës N, Dolbow J, Belytschko T. A finite element method for crack growth without remeshing. *International Journal for Numerical Methods in Engineering* 1999; **46**:131–150.
8. Stolarska M, Chopp D, Moës N, Belytschko T. Modelling crack growth by level sets in the extended finite element method. *International Journal for Numerical Methods in Engineering* 2001; **51**(8):943–960.
9. Belytschko T, Chen H. Singular enrichment finite element method for elastodynamic crack propagation. *International Journal of Computational Methods* 2004; **1**(1):1–15.
10. Menouillard T, Belytschko T. Dynamic fracture with meshfree enriched XFEM. *Acta Mechanica* 2010; **213** (1–2):53–69.
11. Hughes TJR, Cottrell JA, Bazilevs Y. Isogeometric analysis: CAD, finite elements, NURBS, exact geometry and mesh refinement. *Computer Methods in Applied Mechanics and Engineering* 2005; **194**(39-41):4135–4195.
12. Benson DJ, Bazilevs Y, Hsu MC, Hughes TJR. A large deformation, rotation-free, isogeometric shell. *Computer Methods in Applied Mechanics and Engineering*; in press, DOI: 10.1016/j.cma.2010.12.003.
13. Benson DJ, Bazilevs Y, De Luycker E, Hsu MC, Scott M, Hughes TJR. A generalized element formulation for arbitrary basis functions: from isogeometric analysis to XFEM. *International Journal for Numerical Methods in Engineering* 2010; **83**(6):765–785.
14. Lipton S, Evans J, Bazilevs Y, Elguedj T, Hughes TJR. Robustness of isogeometric structural discretizations under severe mesh distortion. *Computer Methods in Applied Mechanics and Engineering* 2010; **199**(5-8):357–373.
15. Bazilevs Y, Calo V, Cottrell J, Hughes TJR, Reali A, Scovazzi G. Variational multiscale residual-based turbulence modeling for large eddy simulation of incompressible flows. *Computer Methods in Applied Mechanics and Engineering* 2007; **197**(1-4):173–201.
16. Bazilevs Y, Calo VM, Hughes TJR, Zhang Y. Isogeometric fluid–structure interaction: theory, algorithms, and computations. *Computational Mechanics* 2008; **43**(1):3–37.
17. Akkerman I, Bazilevs Y, Calo V, Hughes TJR, Hulshoff S. The role of continuity in residual-based variational multiscale modeling of turbulence. *Computational Mechanics* 2008; **41**(3):371–378.
18. Elguedj T, Bazilevs Y, Calo VM, Hughes TJR. B-bar and F-bar projection methods for nearly incompressible linear and non-linear elasticity and plasticity using higher-order NURBS elements. *Computer Methods in Applied Mechanics and Engineering* 2008; **197**(33–40):2732–2762.
19. Réthoré J, Elguedj T, Simon P, Coret M. On the use of NURBS functions for displacement derivatives measurement by digital image correlation. *Experimental Mechanics* 2009; **50**(7):1099–1116.
20. Babŭska I, Melenk JM. The partition of unity method. *International Journal for Numerical Methods in Engineering* 1997; **40**(4):727–758.
21. Laborde P, Pommier J, Renard Y, Salaün M. High-order extended finite element method for cracked domains. *International Journal for Numerical Methods in Engineering* 2005; **64**:354–381.
22. Cheng KW, Fries T-P. Higher-order XFEM for curved strong and weak discontinuities. *International Journal for Numerical Methods in Engineering* 2009; **82**(5):564–590.

23. Vitali E, Benson DJ. Contact with friction in multi-material arbitrary Lagrangian–Eulerian formulations using X-FEM. *International Journal for Numerical Methods in Engineering* 2008; **76**(6):893–921.
24. Krongauz Y, Belytschko T. EFG approximation with discontinuous derivatives. *International Journal for Numerical Methods in Engineering* 1998; **41**(7):1215–1233.
25. Belytschko T, Gracie R, Ventura G. A review of extended/generalized finite element methods for material modeling. *Modelling and Simulation in Materials Science and Engineering* 2009; **17**(4):043001.
26. Johnson R. Higher order B-spline collocation at the Greville abscissae. *Applied Numerical Mathematics* 2005; **52**(1):63–75.
27. Auracchio F, Beirão da Veiga L, Hughes TJR, Reali A, Sangalli G. Isogeometric collocation methods. *Mathematical Models and Methods in Applied Sciences* 2010; **20**(11):2075–2107.
28. Hansbo A, Hansbo P. A finite element method for the simulation of strong and weak discontinuities in solid mechanics. *Computer Methods in Applied Mechanics and Engineering* 2004; **193**(33–35):3523–3540.
29. Menouillard T, Belytschko T. Smoothed nodal forces for improved dynamic crack propagation modeling in XFEM. *International Journal for Numerical Methods in Engineering* 2010; **84**(1):47–72.
30. Hughes TJR, Reali A, Sangalli G. Efficient quadrature for NURBS-based isogeometric analysis. *Computer Methods in Applied Mechanics and Engineering* 2010; **199**(5–8):301–313.
31. Fries T-P. A corrected XFEM approximation without problems in blending elements. *International Journal of Solids and Structures* 2008; **75**:503–532.
32. Ventura G, Gracie R, Belytschko T. Fast integration and weight function blending in the extended finite element method. *International Journal for Numerical Methods in Engineering* 2009; **77**(1):1–29.
33. Chessa J, Wang H, Belytschko T. On the construction of blending elements for local partition of unity enriched finite elements. *International Journal for Numerical Methods in Engineering* 2003; **57**:1015–1038.
34. Belytschko T, Moës N, Usui S, Parimi C. Arbitrary discontinuities in finite elements. *International Journal for Numerical Methods in Engineering* 2001; **50**(4):993–1013.
35. Sevilla R, Fernández-Méndez S, Huerta A. NURBS-enhanced finite element method (NEFEM). *International Journal for Numerical Methods in Engineering* 2008; **76**(1):56–83.